FOSTER, MICHAEL D., M.S. Computational Study of RTI – 371, a Positive Allosteric Modulator of the Cannabinoid CB1 Receptor. (2011)
Directed by Dr. Patricia H. Reggio. 70 pp.

It is now recognized that many G-protein-coupled receptors (GPCRs) contain allosteric binding sites for endogenous and/or synthetic ligands, which are topographically distinct from the agonist-binding site, which is known as the orthosteric site. In contrast to the direct effects on receptor function that are mediated by orthosteric ligands, allosteric drugs act by modulating receptor activity through conformational changes in the receptor that are transmitted from the allosteric to the orthosteric site and/or to effector coupling sites.

3β-(4-methylphenyl)-2β-[3-(4-chlorophenyl)isoxazol-5-yl]tropane (RTI-371) has been shown to be a positive allosteric modulator of human cannabinoid receptor type 1 (CB1). RTI-371 increases the affinity of traditional cannabinoid agonist, CP55,940 and boosts its efficacy. These effects suggest that this compound may cause a structural change in the CB1 receptor, such that the intrinsic activity of CP55,940 is enhanced, perhaps by stabilizing the active conformation of the receptor. RTI-371 has also been reported to be devoid of activity in the absence of agonist, making RTI-371 neither an agonist nor an antagonist at CB1 when applied alone.

The goal of this thesis project was to understand the action of RTI - 371 at the molecular level. To this end, five specific aims were pursued. First, a complete Jaguar conformational analysis of RTI-371 was accomplished, establishing both the minimum

energy conformations and the global minimum energy conformation of RTI-371. Second, to identify the binding site of RTI-371 at CB1, the forced-biased Metropolis Monte Carlo simulated annealing program (MMC) was employed. Third, because an increase in CP55,940 affinity could be achieved by receptor exit route blockade, the program CAVER was used to identify all exit routes and the most likely exit route for CP55,940 from CB1. Fourth, the results of MMC and CAVER were used to identify the most likely binding site region for RTI-371 at CB1. Fifth, binding sites for RTI-371 in this region of the receptor were explored using an automated docking program Glide. The most favorable binding site identified for RTI-371 at CB1 is consistent with the reported pharmacology of RTI-371, i.e., its ability to boost CP55,940 affinity and efficacy through stabilizing the active state of CB1 receptor.

COMPUTATIONAL STUDY OF RTI – 371, A POSITIVE ALLOSTERIC MODULATOR OF THE CANNABINOID CB1 RECEPTOR

by

Michael D. Foster

A Thesis Submitted to
the Faculty of The Graduate School at
The University of North Carolina at Greensboro
in Partial Fulfillment
of the Requirements for the Degree
Master of Science

Greensboro
2011

Approved by

_____
Committee Chair

APPROVAL PAGE

This thesis has been approved by the following committee of the Faculty of The Graduate School at The University of North Carolina at Greensboro.

Committee Chair _____
Dr. Patricia H. Reggio

Committee Members _____
Dr. Alice E. Haddy

_____
Dr. Liam M. Duffy

_____
Date of Acceptance by Committee

_____
Date of Final Oral Examination

TABLE OF CONTENTS

LIST OF TABLES

Page

LIST OF FIGURES

Page

CHAPTER I

INTRODUCTION

G protein-coupled receptors (GPCR) have been a mainstay in the pharmaceutical industry and currently two thirds of pharmaceutical research programs are based on agents that act at these receptors [1]. GPCRs are a superfamily of receptors, with >800 members, regulating many cellular signal transduction events such as differentiation, proliferation, angiogenesis, cancer, development, and cell survival [1]. However, not limited to transduction, GPCRs are also responsible for other types of communication across the plasma membrane. In higher organisms, these receptors are responsible for the recognition of environmental stimuli such as light, taste, and odor.

The goal of this thesis project is to understand the action of the novel allosteric modulator, 3β-(4-methylphenyl)-2β-[3-(4-chlorophenyl)isoxazol-5-yl]tropane (RTI - 371) at the hCB1 (human cannabinoid receptor type 1). Typically found in the central nervous system, hCB1 is a Class A GPCR. GPCR's are broken into six classes based on sequence homology and functional similarity, with Class A referring to "rhodopsin like" in structure [2]. In 1990, CB1's amino acid sequence was found to be consistent with the tertiary structure of a GPCR, subsequently, the complimentary DNA of CB1 was cloned and expressed by Matsuda and co-workers from a rat cerebral cortex cDNA library [3].

The primary amino acid sequence of an N-terminus variant of CB1 and the sequences for human and mouse CB1 have also been reported [4, 5].

Since the initial x-ray crystal structure for bovine rhodopsin (PDB#1U19) was solved, it has served as a standard for studying GPCR's. However, recently, several new x-ray crystal structures for GPCR's have been published. These include the β_2-adrenergic receptor (β_2-AR) [6-8], β_1-adrenergic receptor (β_1-AR) [9], adenosine A2A receptor [10] and most recently the CXCR4[11] and dopamine D3 [12] receptors. Although the general topology is the same between these structures, there are some local differences dictated by the sequences within these receptors.

General G-Protein Coupled Receptor Structure

The generalized structure of GPCR's include seven transmembrane alpha helices (TMHs) connected by intervening loops with an extracellular N-terminus and an intracellular C terminus that begins with a short helical segment (Hx8) oriented parallel to the membrane surface [1]. (Figure 1) Historically, the uses of rhodopsin as a template for the development of models of other Class A GPCRs have been important. Sequence alignments with rhodopsin were made by aligning highly conserved residue positions (e.g., N1.50, D2.50, W4.50 and P5.50) and highly conserved motifs (e.g., D/ERY in TMH3, CWXP in TMH6 and NPXXY in TMH 7). This then enabled the identification of regions with secondary structures such as helices and loops.

Figure 1: Generalized structure of a G-protein coupled receptor.

Palczewski and coworkers first reported the x-ray crystal structure bovine rhodopsin in the dark (inactive) state (PDB #1F88) [13]. Structurally, a total of 338 amino acid residues corresponding to 97.1% of the opsin molecule were resolved, with the last 15 residues of the C-terminus modeled as alanines. Also resolved in the structure was the 11-cis-retinal chromophore (covalently bound to K(296)), as well as two zinc ions, three mercury ions and several water molecules[13]. Rhodopsin is understood to be opsin (PDB#3CAP) [14] bound with 11-cis-retinal. Isomerization of 11-cis-retinal to all trans-retinal is initiated by absorption of a photon, leading to a conformational change in

the receptor that permits coupling to the G protein (transducin) and subsequent signal transduction[13].

As detailed by Hanson, the 2008 publication of the ligand-less opsin structure at 2.9 Å and opsin bound to a peptide from transducin (the main conduit by which rhodopsin transmits signaling information) at 3.2 Å pushed the understanding of GPCR's closer to resolving the active form of the receptor [15]. No significant structural differences were seen upon binding of opsin to the C-terminal peptide from transducin, suggesting that in the absence of its covalently bound ligand (11-cis-retinal) opsin establishes an equilibrium close to that of an activated receptor that is capable of binding with its signaling partner [15].

Unique from the opsin / rhodopsin, recent structural evaluations adenosine A2A (PDB#3EML)[10], β-1-adrenergic (PDB#2RH1)[16], and β-2-adrenergic (PDB#2VT4) [9], Chemokine receptor type 4 (CXCR-4) (PDB#3ODU) [17], and dopamine D3 receptor (PDB#3PBL) [18] receptor were released. In one structure, A2A ,the ligand is bound in a different orientation than expected based on rhodopsin [15]. The bound ligand orientation was one difference, however, to adequately compare newer released structures of Class A GPCR's one must consider structural uniqueness, outside of the binding pocket, in the other main areas such as the extracellular loops, transmembrane helices, and intracellular loops.

Extracellular Region

Structural comparisons, within the extracellular regions, reveal differences across the rhodopsin family of receptors. Overall, looking at images with the ECL region expanded to create a surface view (Figure 2), rhodopsin, βAR's, A2A, CRCX-4, and dopamine D3 reveal how different the levels of occlusion to the binding ligand the binding pocket can be. Immediately, rhodopsin's binding pocket is seen to be completely occluded (Figure 2A), while the others are only partially. While occlusion can be seen in the surface view of the ECL region, differences in the secondary structures for each receptor can be better compared by looking at the receptors from the same top down perspective from a structural view (Figure 3). Structurally, in this region, rhodopsin has one disulfide bridge, essential for normal function, and extensive secondary and tertiary structures occluding the ligand-binding site from fragment [15, 19]. Comparatively, βAR's extracellular regions are open lacking interaction between ECL3 with ECL1 or ECL2 [15]. This partial occlusion is due primarily to a helical segment within ECL2 that is supported by interaction with ECL1 and secondarily to a random coil section of ECL2 formed at the top of the ligand-binding pocket. Besides being less occluded from fragment, the βAR's ligand-binding pocket is also more constrained because it has two disulfide bridges, one fixed with a random coil segment on ECL2, C-terminal to the helical stretch, and the other attaching the entire loop to the top of TMH3 at C3.25 [15]. Differing from rhodopsin and βAR's, in the extracellular region among the 3 loops A2A is highly constrained by four disulfide bridges (Figure 3C) and multiple polar and van der

Waals interactions [15]. Three of the four disulfide bridges serve to stabilize a short helical segment of ECL2, N terminal to TMH5, by anchoring it to ECL1 and the top of TMH3 [15]. This constrained pocket allows access to two residues, F(168) and E(169), important for ligand binding interactions [15]. Contributing to the structural constraint, A2A has multiple ligand binding interactions because its ECL3 contains an intraloop disulfide bridge between C(259) and C(262). The disulfide bridge is speculated to constrain the position of H(264), which forms a polar interaction with E(169).

A) Rhodopsin Receptor **B) β-Adrenergic Receptor** **C) Adenosine A2A Receptor**

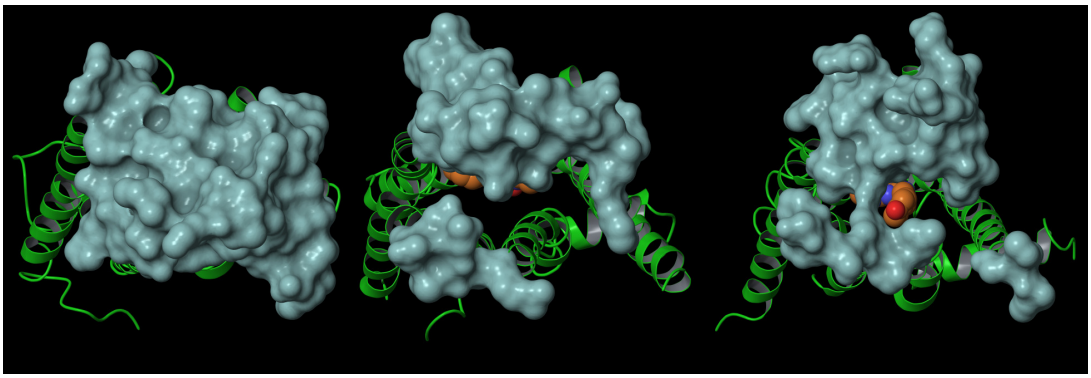

D) CXCR-4 Receptor **E) Dopamine D3 Receptor**

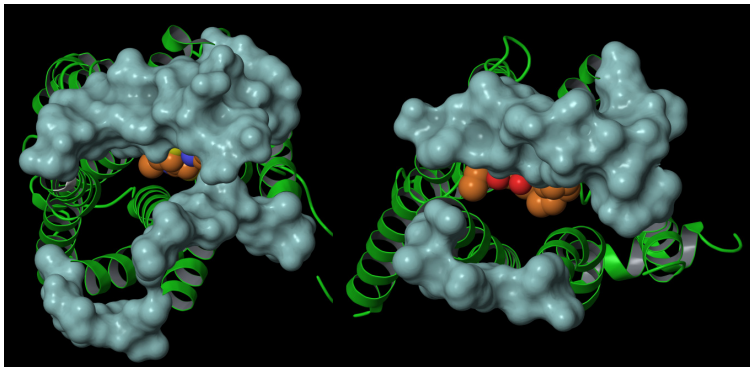

Figure 2: Expanded surface view of extracellular View of Rhodopsin, β-Adrenergic, Adenosine A2A, CXCR-4, and Dopamine D3 Receptors showing different levels of occlusion to the ligand binding pocket. The orthosteric ligands are in VDW with orange carbons, extracellular loops in VDW surface view, and the remainder of the receptors in green.

Similarly, CXCR4 and D3 (Figure 3D, E) show a conserved ECL3 cysteine in the extracellular region [12, 20]. Mutation studies have revealed that these cysteines play a role in a more involved and coordinated interaction occurring between ECL3 and N terminus that is essential for receptor signaling [20]. It has also been suggested that the disulfide linkage at the ECL3 - N terminus interface might serve as a "microswitch" in rhodopsin family receptors and these cysteine pairs might be acting as redox sensors

responding to peroxides, reactive oxygen species, reducing agents, or enzymes that modify the disulfide bridges such as protein-disulfide isomerases [20].

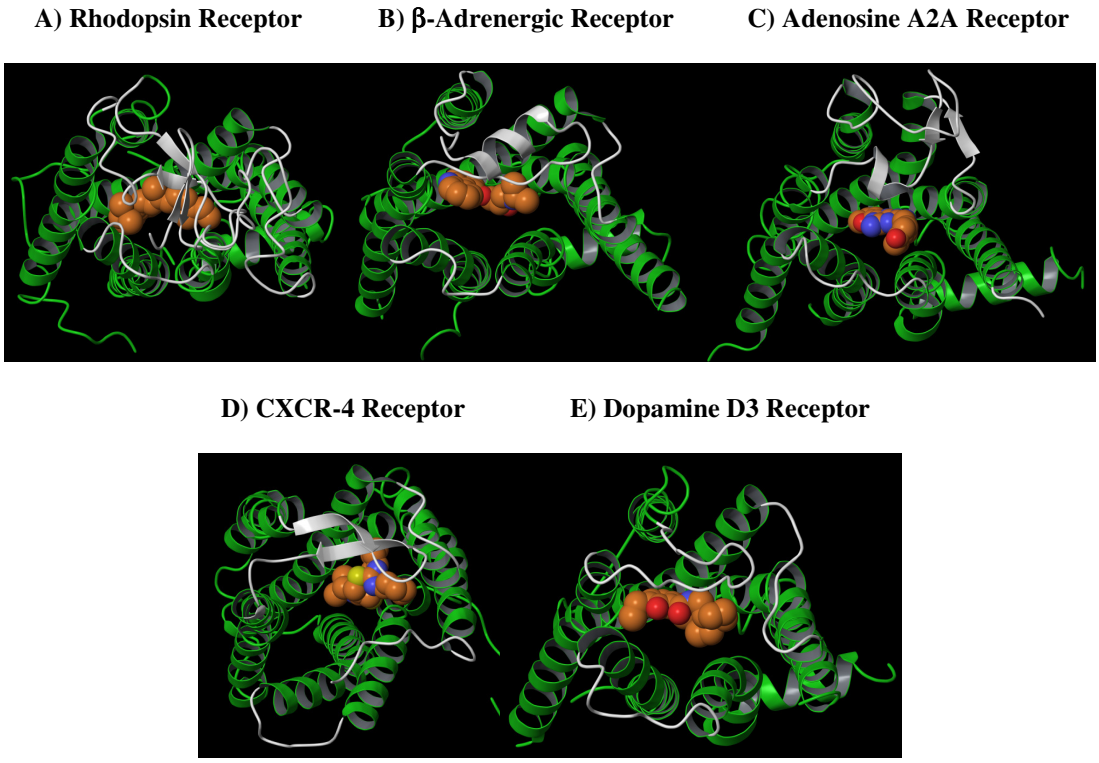

Figure 3: Extracellular View of Rhodopsin, β-Adrenergic, Adenosine A2A, CXCR-4, and Dopamine D3 Receptors showing structural features. The orthosteric ligands are in VDW with orange carbons, binding pocket with extracellular loops in white, and the remainder of the receptors in green.

In D3, the second extracellular loop (ECL2) is shorter than in the βARs which also lack the helical secondary structure [12]. However, the portion of ECL2 in D3 (residues 182 to 185) that contributes to the ligand binding pocket is quite similar to the βARs by way of spatial positioning relative to the bound ligand and location of side chains in the binding pocket [12]. Constraining the position of ECL3 and orienting

H(359) at the top of the ligand binding site is a disulfide bond between C(355) and C(358) in ECL3 in addition to the canonical disulfide bond bridging ECL2 C(181) and helix III C3.25 [12]. A similar intraloop disulfide bond to D3 is present in the A2A structure.

With all of the differences in the extracellular region highlighted, one similarity is seen, the entire 28-residue N terminus is completely disordered in rhodopsin, βARs, and A2A's [15]. Following the same, the 31-residue N terminus for D3 and 26 – residue N terminus for CXCR4 structures solved to date are also reported to be completely disordered [12, 17].

Transmembrane Helices

Ye and Godzik used the high residue conservation among class A GPCRs within the transmembrane helical regions, to perform a sequence alignment of these regions for five representative GPCRs [15, 21]. In this work, the core regions were determined using a PYMOL structural alignment algorithm and the total transmembrane RMSD was calculated using LSQMAN [15]. Evaluation identified a common structural core of 97 residues completely conserved with an average Cα RMSD of 1.3 Å, yielding the sequence conservation expected [15]. Also reported, unlike the core residues, the non-core residues tend to be highly structurally divergent, increasing the total transmembrane RMSD considerably to 2.1 to 2.8 Å [15].

One of the important structural features conserved for the βARs and A2A structures and all Class A receptors, within the transmembrane helix region, is a triplet of

residues termed the D/ERY motif [15]. This motif, consisting of an aspartate or glutamate followed by an arginine and tyrosine, is near the intracellular end of TMH3 found in most class A GPCRs. This motif is recognized in rhodopsin to take part in a conserved interaction referred to as the "ionic lock", with a glutamate residue at the base of TMH6 (D/E6.30) [13, 15, 22, 23]. However, despite the presence of the D/ERY motif and glutamate residue, no ionic lock interaction is reported to be observed in the structures of the βARs and A2A [15]. This suggests that either the ionic lock observed in rhodopsin is not a universal interaction among the class A receptors or more likely that the functionalization of the βARs and A2A in their IC3 loops to achieve crystallization may have perturbed the structure of the ionic lock. Of the receptors shown the only one to have an intact ionic lock is rhodopsin. (Figure 4)

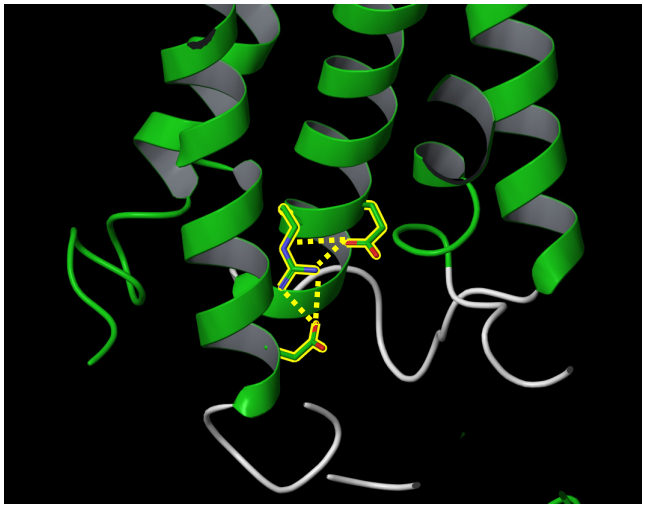

Figure 4: "Ionic lock" interaction between R (3.50) of the D/ERY motif and D (6.30).

Ligand Binding Pocket

Continuing a comparison of structural differences and similarities the binding pocket can be explored. Comparison of βARs and A2A's binding pocket with rhodopsin highlight an area of uniqueness between the two.(Figure 5) For βARs, the position of binding pocket is very similar to rhodopsin and does not vary considerably with alternate ligands or between different subtypes of different species [9, 15, 16, 24]. As previously stated, however, the same does not appear true for A2A. As shown in Figure 5A and 5B, the aliphatic tail of carazolol, a representative ligand (bound in βAR) follows a very similar path as that of retinal (bound in rhodopsin) extending from TMH7 to the TMH5/6 interface. Similar, but not identical, the positions of retinal and carazolol in the binding pocket deviate, as retinal extends deeper into the receptor and interacts with W6.48 (generally conserved in class A receptors and thought to be involved in receptor signaling) [15, 24]. Carazolol does not extend far enough for interaction, however, does appear to form more extensive interactions with TMH5 [15]. Differently, the binding position of A2A's ligand (ZM241385) is reported to be shifted and rotated to the interface of TMH6 and TMH7 [25]. This change allows the longest axis of ZM241385 to be positioned perpendicular to the defined plane of the plasma membrane and facilitates extensive interactions with the ECL2, creating a bulk fragment exposed ligand slightly higher in A2A's binding pocket (Figure 5C) [15].

A) Rodopsin Receptor **B) β-Adrenergic Receptor** **C) Adenosine A2A Receptor**

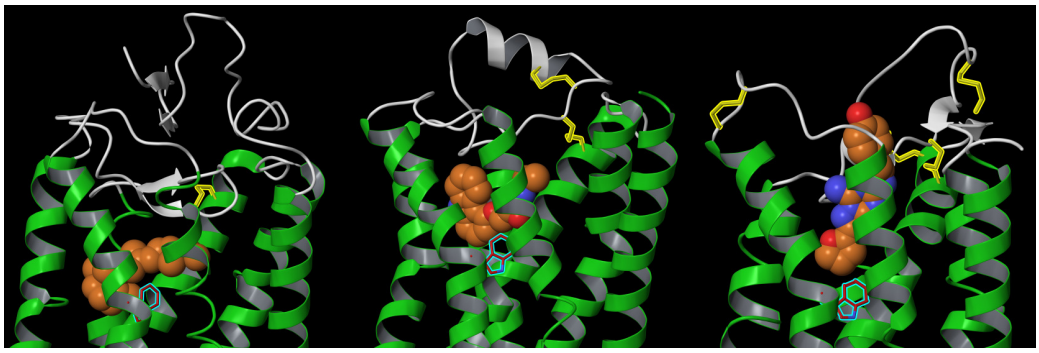

D) CXCR-4 Receptor **E) Dopamine D3 Receptor**

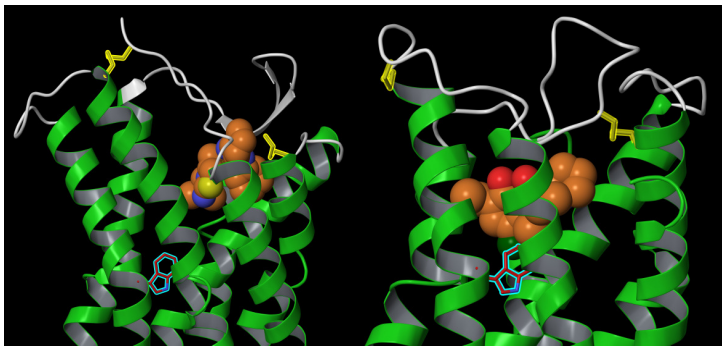

Figure 5: Side view of orthosteric ligand binding pocket and extracellular loop region of Rhodopsin, β-Adrenergic, Adenosine A2A, CXCR-4, and Dopamine D3 Receptors. Internal disulfide linkages highlighted yellow, orthosteric ligands in VDW with orange carbons, and conserved tryptophan "toggle switches" in red/blue.

Intracellular Loops

The intracellular loop regions are structurally important and changes within them have been associated with differences in basal activity for GPCRs [15, 25]. In the βARs and A2A receptors, the TMH3 D/ERY region interacts with ICL2 by means of a polar hydrogen bond between the aspartate residue and either a serine or tryptophan resident on the loop [15]. A2A and β1AR have low basal activity and their ICL2 consists of a short

helical segment with the DRY aspartate reportedly interacting with the conserved tyrosine on TMH3 [15, 26, 27]. However, when the DRY aspartate interacts with a serine two positions C terminal to the conserved tyrosine, as in β2AR, this change is correlated with high basal activity, suggesting an influence that structural features of the intracellular loop region may have on GPCRs [15, 26]. Highlighting other structural differences in the region, rhodopsin's TMH5 is reported to extend one turn below the plane of the membrane, however, upon loss of retinal, TMH5 becomes extended by two turns [15, 28]. This change shortens ICL3 and possibly constrains the movement of TMH6, pulling it outward and away from the base of TMH3 and the DRY motif [15].

Recently released, Chemokine receptor type 4 (CXCR-4) and dopamine D3 receptor, show changes in each of the regions from the model based heavily on rhodopsin, but also contain similar functionalization of the EC3 loop. The details of these 5 new structures with a comparison of rhodopsin / opsin structures will be considered when evaluating critical interaction sites for class A GPCR's and determining influence on modulatory activity. However, while understanding the structures of newer GPCR's is critical, establishing effects a compound will have on modulatory activity requires a review of current understanding of activation of a receptor for ligand binding.

GPCR Signaling

It is accepted that GPCR's can exist in at least two states, the inactive (R) state and the activated (R*) state. The pharmacology of GPCRs has been based largely on two-state receptor models [29, 30]. In a two state model, activation is driven by a shift in

the equilibrium between distinct conformations (active and inactive) of the receptor. Accordingly, constitutive activity is explained by an agonist-independent conversion from an inactive (R) state to an active (R*) state [30, 31]. The simple two-state model, however, is being challenged by biochemical data showing that an activated receptor is often capable of coupling to a number of heterotrimeric G proteins, and that different signaling cascades can be activated from a single receptor depending on the nature of the bound agonist [31]. This, in turn, implies that there may be more than one activated state of a GPCR.

In the ternary complex model, the ternary complex consists of the receptor (R), agonist (A), and the G protein (G). To help explain this model, Park and co-workers published a qualitative evaluation of typical patterns revealed through competition binding studies [30]. Using a fixed concentration of a radiolabeled antagonist and graded concentrations of an unlabeled agonist, curves yielding Hill coefficient data were generated [30]. Upon evaluation, the corresponding curves, suggested that results of agonist binding assays could be attributed to two interconvertible states of the receptor that coexist in equilibrium in the absence of guanyl nucleotides and bind to agonists with different affinities [30]. The investigators reported that activation of the receptor is dependent on its ability to form a complex with the G protein, furthering the concept that coupling of the receptor to the G protein (RG) results in an active state of the receptor that binds agonist with high affinity, whereas the uncoupled receptor (R) is inactive and exhibits low affinity for agonist [30].

Activation using a heterotrimeric protein model suggests the ability to have inactive R state with an activated R* state facilitating the existence of multiple conformational states [31]. A heterotrimeric protein model based on using homo and heterodimers of GPCRs that incorporates active and inactive states is not necessary for evaluating modulation of ligand binding. Since ligands can be thought to bind after a receptor is in an active R* state, evaluating how a compound modulates an active state receptor only requires the monomeric R* state. For that reason, a monomeric GPCR model based on a homology structure of a well studied protein, such as rhodopsin, was used in the work reported here.

A model of the activated state of the CB1 receptor has been built by the Reggio lab based on conformational changes that have been suggested to occur via biophysical studies of rhodopsin and the β2 adrenergic receptor [32-37]. To accomplish this, two mechanisms have been shown to be important in transitioning from an inactive state: (1) rigid domain movements of transmembrane helices that result in changes in the intracellular domains and (2) movement in the ligand binding pocket. Biophysical studies of rhodopsin and the β2 adrenergic receptor have suggested that activation is accompanied by counterclockwise (from an extracellular view point) rotations of TMH3 and TMH6 [32, 38, 39]. A E3.49/R3.50/E6.30 salt bridge constrains the intracellular, cytoplasmic end of TMH3 and TMH6. P6.50 of the highly conserved TMH6 CWXP motif acts as a hinge allowing TMH6 to straighten, moving its intracellular end away from TMH3 and up toward the lipid bilayer [35, 40]. Facilitating the transition to the

activated state, the ionic lock is broken and subsequent protonation of E3.49 occurs. [13, 32, 41, 42] A CB1 receptor model, based on the above information, tested through mutation [43, 44], substituted cysteine accessibility [45], and covalent probe experiments [46] was built and refined in the Reggio lab.

Besides movements in the intracellular domains, another aspect of GPCR activation is a toggle switch that exists in the binding pocket [47]. The "rotamer toggle switch", involving W6.48 on TMH6 [44, 47, 48], is believed to be a non-covalent interaction, in the basal state of a GPCR, that must be changed to migrate from the inactive to the active state. In mapping the process of changing from the dark inactive state of rhodopsin to the light activated state, the beta-ionone ring, of 11-cis-retinal, close to W6.48 (which is in a χ_1 = g+ state) of the CWXP motif on TMH6, moves away from TMH6 towards TMH4, where it locates near A4.58 [49]. This movement releases any constraints on W6.48, making it possible W6.48 to undergo a conformational change. Biophysical studies have shown that perturbations in the environment of W6.48 of rhodopsin occur during the conformational change concomitant with receptor activation [34]. For rhodopsin, then, the beta-ionone ring acts as a lynch pin, constraining W6.48 in a χ_1 = g+ conformation [13, 50, 51]. This suggests that the conformation of W6.48 when rhodopsin is in its inactive / ground state (R; χ_1 = g+) changes during activation (i.e., W6.48 χ_1 g+ $\rightarrow$ trans) [48].

Correlating to the rotamer toggle switch in rhodopsin is the residue movement in CB1 that creates the "lynch pin" effect. A microdomain of aromatic residues that face

into the ligand binding pocket of CB1 in the TMH3-4-5-6 region, including F3.25, F3.36, W4.64, Y5.39, W5.43 and W6.48, have been studied using the biased Monte Carlo/simulated annealing technique of Conformational Memories combined with receptor modeling. The F3.36(200)/W6.48(356) interaction in CB_1 was shown to correlate to the 11-cis-retinal/W6.48 interaction in the rhodopsin dark state and may serve as the "toggle switch" for CB_1 activation, with F3.36 $\chi 1$ *trans* / W6.48 $\chi 1$ *g+* representing the inactive (R) and F3.36 $\chi 1$ *g+* /W6.48 $\chi 1$ *trans* representing the active (R*) state of CB_1 [52]. Supporting this, a mouse CB_1 F3.36A mutant was shown to exhibit statistically significant levels of in ligand-independent stimulation of GTPγS binding vs. WT mCB_1. Since, basal levels for the W6.48A mutant were not statistically different from WT mCB_1 the results suggested that F3.36 may restrain W6.48 from moving to an active state conformation in the CB1 receptor [44]. Evaluating the counterclockwise motion of the TMH3 and TMH6 during activation would show that W6.48 moves toward TMH5 and F3.36 moves toward TMH2. This motion allows these primary two residues to move past each other.

Domain motion of the ECL2 loop

Previous studies have demonstrated that the conserved disulfide bridge that connects the ECL2 to TMH3 is essential for membrane expression, ligand binding, and G protein activation [53-57]. CB1 lacks the conserved disulfide bridge found in approximately 90% of GPCRs, however, the ECL2 domain motion still plays a role in regulating receptor activation [58]. The ECL2 domain tolerates multiple amino acid

substitutions which can alter side chain character and confer ligand- independent signaling, acting like a negative regulator of receptor activation [58]. This occurs because the ECL2 forms an antiparallel β sheet contacting each of the transmembrane helices and all of the extracellular segments when in the inactive state [58]. Mutation studies and NMR studies offer evidence that displacing the ECL2 is a necessary motion leading to an activated receptor [58, 59]. Solid-state 13C NMR was utilized to measure the distance between a retinal chromophore and β4 strand of ECL2 offering justification to this movement upon activation [59]. Retinal isomerization triggers a helix motion that displaces the loop from the retinal binding site[59]. Light induced structural changes in ECL2 are coupled to the motion of TMH5 when the ionic lock is broken, regulating activation [59]. The crystal structure of rhodopsin shows that the β-strands in ECL2 are extensively knit together by hydrogen-bonding interactions that extend to Y(268) on TMH6 and D(113) on TMH3 [50, 60]. Ultimately, the motion of ECL2 is coupled to the motion of TMH5 and the P(170) – P(171) sequence at the TMH4-β3 boundary serves as a hinge that links β3 to TMH4 and TMH4 to TMH5 [59]. Subsequently, a rearrangement in the hydrogen bonding networks connecting ECL2 with the extracellular ends of TMH4, 5, and 6 displaces the ECL2 from the binding pocket allowing activation [59]. Based on the evidence of its role in activation, it will be critical to avoid interfering with the ECL2 motion when identifying any binding locations for RTI-371 on CB1.

G Protein Coupling

The process of a GPCR interacting with a G protein (guanine nucleotide-binding protein) is generically known as G protein coupling. Localized at the intracellular side of the plasma membrane G-proteins interact with rhodopsin as a physiological response to activation [61, 62]. Heterotrimeric G proteins (transducin) are larger assembled proteins made up of the three subunits known as alpha (G_α), beta (G_β), and gamma (G_γ). As a physiological response, light-induced structural changes for rhodopsin are transferred through the interfacial interaction of the receptor and G protein to the nucleotide-binding site on the Gα subunit [61-63]. This change promotes guanosine diphosphate (GDP) (Figure 6A) release, which leads to the formation of a high-affinity complex between rhodopsin and the nucleotide-free Gprotein [61, 62]. Now, induced structural changes in the interface, or activation, between the G-protein subunits and the receptor, allow guanosine triphosphate (GTP) (Figure 6B) binding to the empty nucleotide pocket leading to the disassembly of the heterotrimeric (αβγ) G protein complex into two individual components G_α and $G_{\beta\gamma}$ [61, 62]. This assembly and reassembly allows the exchange GDP for GTP on the G_α subunit. Dissociation and reassembly of the G-protein complex allows rapid response to the activating signal and subsequent return to basal activity levels once the signal has been removed from the system [61]. All G-protein α-subunits possess an intrinsic GTPase activity that enables them to act as time switches, where hydrolysis of the bound GTP to GDP promotes reassociation of the Gα subunit with the Gβγ dimer into the functional G-protein trimer

[61]. Both the free transducin subunits (Gα-GTP and the Gβγ dimer) can then activate second messenger pathways [61]. Through this process the G proteins can then influence changes downstream in a cell.

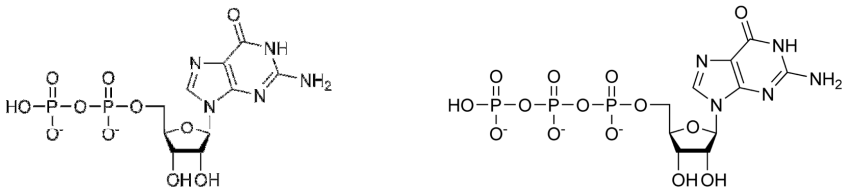

Figure 6: (A) GDP and (B) GTP exchanged on the G_{α} subunit

Structurally the Gα subunit is subdivided into two distinct domains, GTPase and helical domains. The GTPase domain contains a six-stranded β-sheet surrounded by six α-helices arranged with a long central helix surrounded by five shorter helices. Finally, the N-terminal region consists of a long α-helix pointing out from the rest of the Gα subunit [62-64]. The Gβ subunit has a long N-terminal helix followed by a repeating module of seven β-sheets. Each β-sheets has four antiparallel strands, forming a β-propeller structure [62-64]. The final subunit is the Gγ subunit which contains only two helices allowing the N-terminal helix to interact with the N-terminal helix of Gβ, whereas the remaining polypeptide chain of Gγ interacts with the β-propeller structure of Gβ [62-64].

When the hetrotrimeric (αβγ) G protein couples to a receptor (Figure 7), such as rhodopsin, the major sites of interaction on rhodopsin are located on the intracellular side

of the receptor. The main interaction between transducin and rhodopsin occurs between the C-terminal residues of G-alpha and the inner face of TMH6 and the elbow region of Hx8 [61]. This is the side that is closer to the C-terminus (defined by the intracellular view of TMH 1, 2, 6, and 7) and include contributions from the second and third intercellular loops (IL2 and IL3), as well as H8 and the C-terminal tail region [61].

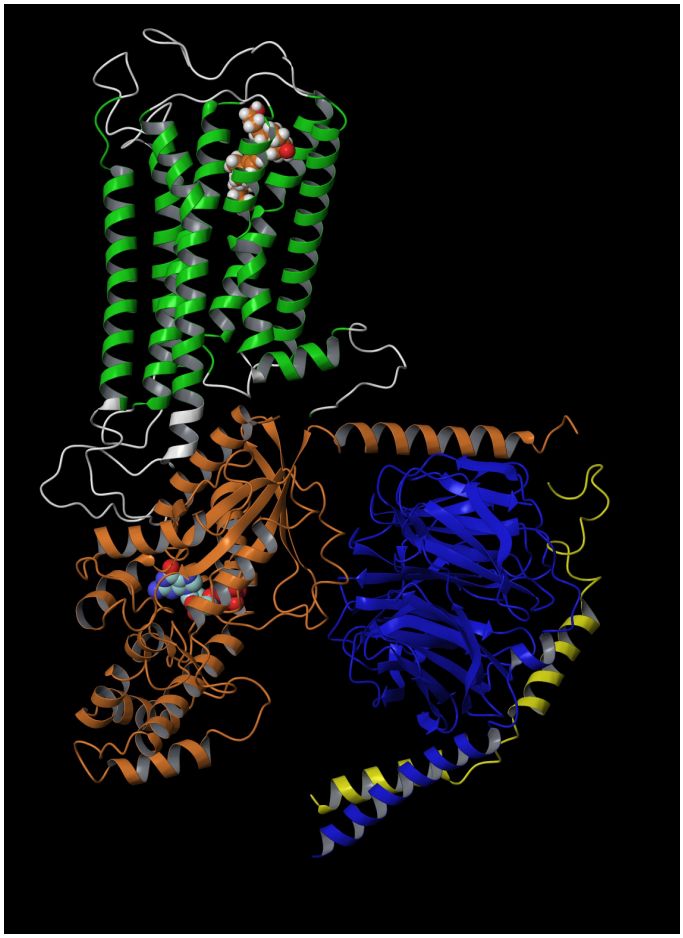

Figure 7: Representation of CB1 R* coupled to a G Protein. Figure shows CB1 R* in Green with orthosteric ligand CP55,940 in VDW with orange carbons. G Protein substituent groups represented as Gα (Orange), Gβ (Blue), and Gγ (Yellow), with GDP present in Gα. CB1 R* modeled in Reggio Lab and G Protein obtained from PDB: 1GG2 [65].

Studies using molecular dynamics simulations to explore interactions between G protein and rhodopsin reveal details that support the experimental results. [61] As previously stated, this interaction is facilitated during activation of rhodopsin by breaking the salt bridge serving as the ionic lock to provide an intracellular opening in the protein that allows the flexible C terminus of Gα to insert into the opened receptor [61-63, 66]. Within this interaction with the receptor the residues known to participate in G-protein binding for rhodopsin are 66-68 on ICL1, 225–227 of ICL3, 235–245 of ICL3 and TMH6, and 312–323 of Hx8 [61, 67]. Furthermore, T(79), located on the cytosolic extension of TMH2 of rhodopsin, also interacts with F(350) on the C-terminus of Gα, while Hx8 engages the C-terminus of Gα through Q(312) [61]. Besides interacting with Gα, rhodopsin also interacts with Gβ [61]. Gβ interactions with rhodopsin, which are accommodated by Hx8 and the C-terminus, take place within three loops of the β-propeller domain, located on the first and last WD-40 units, forming a continuous surface on the side of the molecule that faces the membrane bilayer and the αN helix of Gα [61]. These sites engage the flexible C-terminal region of rhodopsin in the 323CGK motif that follows Hx8, as well as the 334ASTTV and 342SQ motifs [61]. Despite the several reported interaction sites between rhodopsin and transducin, no significant interaction is reported between rhodopsin and Gγ, which is reported to be at a distance more than 10 Å from rhodopsin and oriented on the side of the complex that faces Hx8 [61].

Ligands that interact with CB1 Receptor

The CB1 receptor has five structurally distinct classes of ligands it can interact with. The structures of these ligands are illustrated in Figure 8, while Table 1 summarizes binding interactions for each class. The five classes include classical cannabinoid agonists, such as (6aR)-trans-3-(1,1-dimethylheptyl)6a,7,10,10a-tetrahydro-1-hydroxy-6,6-dimethyl-6H-dibenzo[b,d]pyran-9-methanol), HU-210; non classical cannabinoid agonists, such as (1R3R4R)-3-[2-hydroxy-4-(1,1-dimethylheptylphenyl]-4-(3-hydroxy-propyl)cyclohexan-1-ol, CP55,940; the endogenous cannabinoid agonists, such as, *N*-arachidonoylethanolamine, anandamide; the aminoalkyindole (AA1) agonists, such as 2,3-dihydro-5-methyl-3-[(4-morpholinyl)pyrrolo-[1,2,3-*de*]-1,4-benzoxazin-6-yl](1-naphyl)methanone, WIN55212-2, and diaryl pyrazole antagonist/inverse agonists, such as *N*-(piperdin-1-yl)-5-(4-chlorophenyl)-1-(2,4-dichlorophenyl)-4-methyl-1*H*-pyrazole-3-carboxamide; SR141716A.

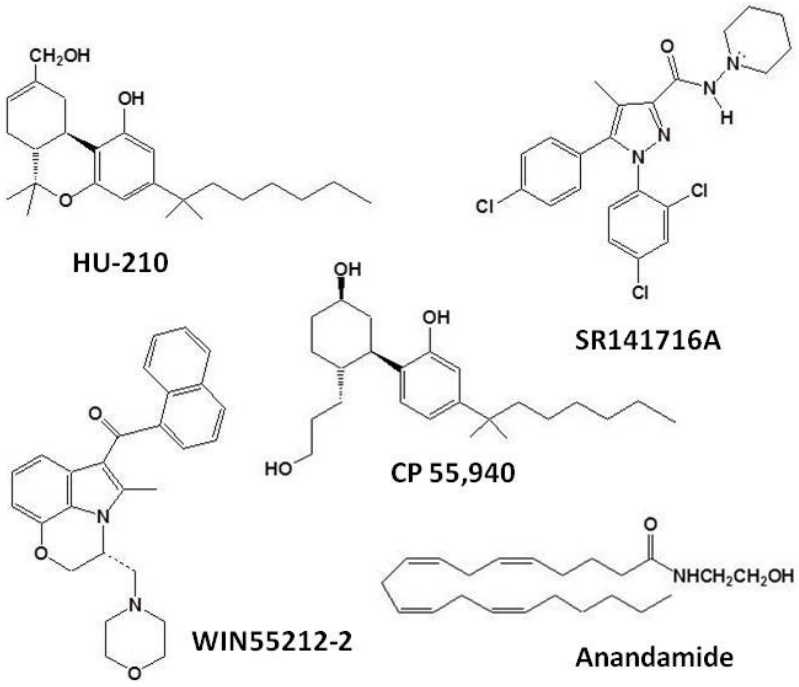

Figure 8: Examples of the five distinct classes of ligands that interact with hCB1.

Individually looking at the classes (Table 1) reveals that four of the five are agonists, which show preference for the active (R*) state and only SR141716A is an inverse agonist/antagonist showing preference to the inactive (R) state. The identified binding regions for these five ligand classes, TMH 2-3-6-7 and TMH 3-4-5-6, further define the binding pocket locations identified using a rhodopsin based CB1 receptor model and can be further defined by the specific binding site location and state of CB1 to which each of the five structural classes bind. (Table1) These binding sites were identified using mutation, cross-linking studies, and computer modeling [43, 44, 68-73].

SR141716A and WIN55212-2, being highly aromatic compounds, have been shown to bind in the TMH 3-4-5-6 region of CB1 [68]. However, these ligands favor different states of CB1. SR141716A is an inverse agonist, having higher affinity for the inactive (R) state, and WIN55212-2 is an agonist, having higher affinity for the activated (R*) state. SR141716A has been shown to form aromatic stacking interactions with F3.36, Y5.39, and W5.43 [44] and a hydrogen bond with K3.28 [70]. Shown to be the key interaction which imparts the SR141716A preference for the R state, this hydrogen bond with K3.28 is only available to the TMH 3-4-5-6 region of CB1 in the inactive state[69, 70].

Mutation studies of K3.28 to alanine in CB1 resulted in a complete loss of binding and a >100-fold decrease in EC_{50} for HU210, CP55,940 and anandamide, however, the affinity of WIN55212-2 was unchanged [71, 72]. These results suggest that the binding site of WIN55212-2 diverges somewhat from that of the classical and endogenous cannabinoids. Experimental and modeling studies have suggested that WIN55212-2 has direct interactions with F3.36, W5.43, and W6.48 in the CB1 R* state [44].

Table 1: Five structural classes of ligands that can interact with CB1 and their corresponding binding pocket.

Class	Example	Binding Site	Interaction Site Residues
Classical agonist	HU-210	TMH 2-3-6-7 region of CB1 in R* [71, 72]	K3.28(192) [71, 72]
Non classical agonist	CP55,940	TMH 2-3-6-7 region of CB1 in R* [43]	K3.28 (primary) S1.39 and K(373) (secondary) [43]
endogenous agonists	anandamide	TMH 2-3-6-7 region in CB_1 R* (U shaped conformation) [68, 73]	K3.28 (hydrogen bonded) and S7.39 (hydrogen bonded) F3.25, V6.59, and F7.35 (lipophilic interaction) [68, 73]
aminoalkyindole agonists	WIN55212-2	TMH 3-4-5-6 region of CB1 in R* state [44, 68-70]	F3.36, W5.43, and W6.48 [44, 68-70]
Diaryl pyrazole antagonist/inverse agonists	SR141716A	TMH 3-4-5-6 region of CB1 in R state [44, 68-70]	F3.36, Y5.39, and W5.43 (aromatic stacking) [44, 68-70]

Mutation data has shown that the affinity of CP55,940 is unaffected by the F3.25A, F3.36A, W5.43A or W6.48A mutations[68], suggesting that unlike WIN55212-2, agonist CP55,940, does not bind in the TMH 3-4-5-6 aromatic microdomain. Instead, modeling studies of the cannabinoid agonist, based on mutation data suggest that CP55,940 binds in the TMH2-3-6-7 region of CB1 with a K3.28 hydrogen being the primary interaction site and S1.39, and K(373) serving as secondary interaction sites. Consistent with this, high affinity binding of CP55,940 is destroyed with mutation of S7.39A [43]. This mutation, predicted by modeling, moves the extracellular end of TMH7 into the binding pocket of CP55,940 and prevent its binding at the site described above [43].

CB1 docking studies of the endogenous agonist anandamide AEA in R* state have suggested that anandamide also binds in the TMH 2-3-6-7 region using K3.28 as its primary interaction site [68]. Modeling studies performed by Brizzi and co-workers

showed a U shaped conformation of AEA in the binding site region docked with the aliphatic chain directed toward the intracellular side of the receptor [73]. Facilitating this, the amide oxygen atom of AEA is hydrogen bonded to K3.28, while the hydroxyl group forms a hydrogen bond with S7.39 and the n-pentyl tail of AEA is stabilized by lipophilic interactions with F3.25, V6.59, and F7.35 [73].

Allosteric Modulators

The agonist or antagonist binding pockets in CB1 are called *orthosteric sites*. Many GPCRs also have *allosteric sites* that are "accessory binding sites" allowing for modulation of ligand activity (positive or negative) without competing for the orthosteric binding site. Binding through an allosteric site allows the allosteric ligand to work in concert with the orthosteric ligand increasing or decreasing activity based on the type modulator (positive or negative) and the type of orthosteric ligand (agonist or antagonist) present. Utilizing both allosteric and orthosteric binding sites simultaneously can give the benefit of making a selective orthosteric drug even more selective. Being devoid of activity in the absence of orthosteric ligands, allosteric modulators offer another benefit, a less disruptive way to influence the functioning of biological systems compared to only orthosteric approaches.

RTI-371 - Allosteric Modulator for hCB1

RTI-371 (Figure 9) is one of several 3-phenyltropane analogues screened by Navarro and co-workers as an indirect dopamine agonist for cocaine addiction therapy. While screening of these products showed a poor correlation between stimulation of

locomotion and dopamine transporter (DAT) inhibition, Navarro found that RTI-371 was shown to cross the blood-brain barrier and block cocaine-induced locomotor stimulation [74]. RTI-371 was further evaluated for intrinsic, antagonist and allosteric modulatory activity at the CB1 receptor using a functional assay based on calcium mobilization [74].

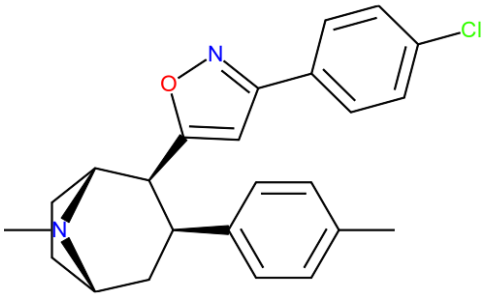

Figure 9: Structural representation of RTI-371

As shown in Table 2, at 10 µM, RTI-371 statistically significantly increased the E_{max} of CP55,940 while lowering its EC_{50} and having no effect on the Hill slope. Summarized in Table 2 and illustrated in Figure 10, the effects of individual compounds on the EC_{50} and E_{max} for CP55,940 were examined. This work showed RTI-371 at 10 $\mu mol \cdot L^{-1}$ but not at 1 $\mu mol \cdot L^{-1}$, increased the efficacy and the potency of CP55,940 and pre-incubation with 10 $\mu mol \cdot L^{-1}$ RTI-370, which is structurally similar to RTI-371, showed the same concentration-dependent effect on efficacy, with 10 $\mu mol \cdot L^{-1}$ causing a 23% elevation in the E_{max} for CP55,940 [74]. Unlike RTI-371, RTI-370 at 1 $\mu mol \cdot L^{-1}$, but not 10 $\mu mol \cdot L^{-1}$ increased agonist potency, however, all findings for RTI-370 were not statistically significant leaving only RTI-371 to be pursued.

Table 2: Effects of Preincubation of CP55,940 on Calcium Mobilization [74].

Compound	CP55,940	RTI-371		RTI-370	
		1 uM	10 uM	1 uM	10 uM
Emax (%) (+/- SEM)	100 (2)	107 (7)	136* (5)	105 (6)	123 (6)
EC50 (nM) (95 % Confidence Interval)	11.4 (10-13)	9.7 (6-14)	4.7* (2-9)	7.9 (5-11)	9.3 (5-17)
Hill Slope (+/- SEM)	1 (0.1)	1 (0.4)	0.9 (0.2)	1.6 (0.5)	1.4 (0.3)

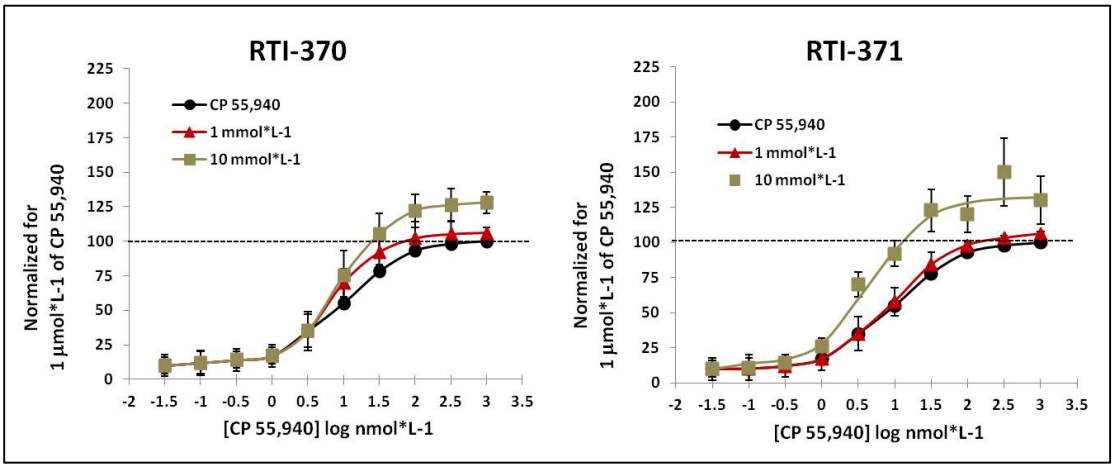

Figure 10: Net fluorescence intensity response curves for CP55,940 in the presence and absence of test compounds (15 min preincubations) [74].

Based on reported positive modulatory activity for CP55,940 and the small change in potency, it is concluded that these compounds cause a structural change in the CB1 receptor, such that the intrinsic activity of CP55,940 is enhanced, by stabilizing the active conformation of the receptor [74]. RTI-371 was also reported to be devoid of activity in the absence of agonist, making RTI-371 neither an agonist nor an antagonist at

CB1 when applied alone [74]. Thus, RTI-371 is a *positive allosteric modulator* of CP55,940 binding affinity and agonist signaling efficacy.

Structure of RTI-371

The structure of RTI-371 includes a tropane ring with two primary substituents: (1) a toluene substituted para to the methyl, and (2) an isoxazole ring linked to para-cholorobenzene. Contrary to the rigidity imposed by the tropane ring, the structure of RTI-371 offers 3 primary rotatable bonds, based on being single, acyclic bonds not attached to a terminal atom, which should provide some conformational flexibility. For this reason, RTI-371 will be studied via computational methods to identify it lowest energy conformation and evaluate the cost of any changes to the minima that would accommodate better binding to CB1.

CHAPTER II

HYPOTHESIS

This thesis tests the hypothesis that RTI-371 is a positive allosteric modulator of CB1 because it blocks the exit of CP55,940 from its orthosteric binding site while not interfering with the extracellular domain motion of EC2 associated with CB1 activation. The region of CB1 that would most likely enable both of the conditions above is a binding site associated with extracellular loops other than the EC2 loop. This hypothesis would support Navarro's conclusion that the proven enhanced intrinsic activity of CP55,940 is realized by stabilizing the active conformation of the receptor [74]. Testing this hypothesis, the following aims were pursued:

Aim 1. Performed a complete Jaguar conformational analysis of RTI-371 at the HF-3-21G* level, establishing all the minimum energy conformations of RTI-371 that were within 2.0 kcal of the global minimum.

Aim 2. Identified sites on CB1 at which the constituent groups present in RTI-371, isoxazole and tropane, would bind using the forced-biased Metropolis Monte Carlo simulated annealing program MMC.

Aim 3. Calculated the most likely exit route for CP55,940 using Caver.

Aim 4. Determine those regions where the results of Aims 2 and 3 intersect.

Aim 5. Using the results of Aim 4, docked RTI-371 at CB1 and evaluated if the EC2 loop remained is unrestrained the allosteric binding site.

CHAPTER III

TECHNIQUES

Conformational Analysis

Conformational analysis was used to establish the available local and global minimum energy conformations of RTI-371. Three primary rotatable bonds were targeted during this conformational analysis and a manual systematic search method [75] and was utilized to ensure that all conformations were identified. Each rotatable bond identified was rotated 360 º in increments of 60 º generating starting points for minimization ensuring the entire conformational space was covered.

Jaguar Optimization

For each starting point, Jaguar based *ab-initio* calculations were employed for the highest level of confidence that all minima were identified. After each rotational increment, the geometry of each resultant rotamer was refined using a Hartree-Fock *ab-initio* geometry optimization at a reasonable basis set level, 3-21G*, using Jaguar [76]. Finally, the resulting conformers for all initial rotamers were examined for uniqueness in structure and ranked according to energy. The global minimum energy conformation was identified from this output. Unique minimum energy conformers that were within 2.00 kcal/mol of the global minimum are considered accessible conformations and retained as

local minima. All conformations in this are considered available conformers when evaluating the docking site for RTI-371 at CB1 (R*) in the presence of CP55,940.

Minimization of CB1 R* with orthosteric ligand (CP55,940)

The wild type CB1 R* bundle with CP55,940 docked was previously prepared in the Reggio group and minimized as described in Kapur et. al. 2007 [43]. This model includes the CB1 transmembrane helix (TMH) bundle, all intra- and extracellular loops, the complete C-terminus and a truncated N-terminus. This ligand/receptor model was used for all calculations described below.

Identification of Allosteric Binding Sites Using MMC

Upon establishing the series of thermodynamically sound conformations for RTI-371, the potential sites for modulation on CB1 was explored via Forced-Biased Metropolis Monte Carlo simulated annealing program (MMC). MMC was utilized because it did not require knowledge of experimental ligand – protein binding thermodynamics, such as multiple-copy-simultaneous search method, MMC does not needing a calibration of known ligand – protein binding energies, such as the linear interaction energy method, and finally MMC is not as time consuming as force-field based approaches [77].

To identify potential interaction sites, the protein was immersed in a simulated field of fragments derived from the compounds, isoxazole and tropane, within the RTI-371 structure. After the protein is completely immersed, the chemical potential was annealed by lowering the system energy, causing only those fragments with the highest

potential to bind to the protein surface to remain [77]. Generally based on Monte Carlo sampling, MMC offers a technique for searching an entire protein surface for sites that yield the lowest free energy of interaction with the protein. Within a defined virtual box, individually the isoxazole and tropane fragments of RTI-371 were sampled in and on the entire surface of CB1. To do this the ensemble started with a system energy that is the excess chemical potential relative to the chemical potential of the reference state [77].

$$\mu - \mu_{ideal} \qquad \textbf{(1)}$$

To establish the reference state, using an ideal gas, $\Delta E = 0$, and $B = 0$ the equation below will yield 1 fragment per system volume V.

$$\frac{P_{ij}}{P_{Ji}} = \left(\frac{V}{N_j}\right) * e^{(B)} * e^{\left(\frac{-\Delta E}{kT}\right)} \qquad \textbf{(2)}$$

To simplify correlation to the chemical potential, referencing it to a unitless term known as a B value is employed in MMC. The following equation shows how the B value is correlated to the excess chemical potential and the concentration of fragment compounds in the system[77].

$$B = \frac{(\mu - \mu_{ideal})}{kT} + \ln([N]) \qquad \textbf{(3)}$$

The B value is the term that is actually annealed with the simulation [77]. Thus, excess chemical potential is based on the number of fragments present in the system [77]. The

annealing process is iterative, so at each B value, the program made a series of attempts to insert and delete molecules into the system until the system equilibrates based on the established B value for that run [77]. Initially, the B value was set to a high number to allow the largest concentration of fragments within the defined space in and around the protein [77]. This started the process of filling the defined box and immersing the protein in fragments. Next, during the run the box fills and the number of fragments remaining has to become stabile, i.e. the box is full. Once the B value is at a stabile point the B value is lowered. Iteratively, the new lower B value starts with the previous B values end results. The process of annealing the B value continues until no fragments remain in the system.

In MMC, fragment molecules and the protein are treated as rigid structures [77]. The only allowed movements for fragments are rotation or translation attempted randomly within the system and entry and exit from the ensemble, all based on the probabilities given by the following equations [77]:

$$\alpha_{insert} = \min\left[1, e^{\frac{\left(\frac{-\Delta E}{kT}+B\right)*V}{(N+1)}}\right} \qquad \textbf{(4)}$$

$$\alpha_{delete} = \min\left[1, e^{\frac{\left(\frac{-\Delta E}{kT}-B\right)*N}{(V)}}\right} \qquad \textbf{(5)}$$

$$\alpha_{move} = \min\left[1, e^{\left(\frac{-\Delta E}{kT}\right)}\right] \qquad \textbf{(6)}$$

For these equations ΔE again refers to the system energy, B is the dimensionless chemical potential, and T is the and temperature of the system [77]. Each equation allows for the corresponding move to be equated to a ΔE that will be positive or negative, with favorable moves resulting in net lower or negative ΔE [77].

For each B value within a run, a defined number of snapshots were taken to evaluate macroscopic changes to system's state related to the free energy given by that B value. Evaluations of each simulation were used to identify a transition point in which the bulk of the fragment compounds left the system and the final B value in which fragment molecules were still present in the system was identified. Output snapshots from the final B value for each of the fragment runs were inspected to visually determine where the fragments preferentially collect. Subsequently runs from isoxazole and tropane were compared to simulations using water as the fragment to verify a favorable displacement.

CAVER

CAVER was developed to identify egress pockets, voids, and cavities in and on the surface of proteins [78]. While understanding that anatomy of tunnels change in time due to the dynamics of a proteins active or inactive state, CAVER was used to select the lowest expense route CP55,940 can use to exit the R* state of CB1.

Identifying the space between molecules in CAVER for complex compounds, such as proteins, requires each element to be represented as a van der Waals sphere and

each measurement of distance to be made from the center of the sphere [78]. The representative spheres are established with a predefined radius based on an AMBER force field in which most of the radii of heavy atoms seen in biomolecules (C, N, O, S, and P) range from 1.6 to 2.1 Å [78]. For proteins, a grid mesh is generated on the surface to provide measurement points for the cost algorithm from the defined starting point. The starting point is the coordinates of the center of mass for CP55,940 in the orthosteric binding pocket of the CB1 model.

Two major drawbacks have been noted for CAVER, very large demands on processor time and memory when used for large channels and small persistent error due to grid extrapolation [78]. While the first is routinely improved with better technology, refinements in the algorithms have dealt with the latter issue. These refinements lead to the use of a three dimensional mesh known as Voronoi facet which is utilized when computing the random search function (Dijkstra's algorithm), selecting the shortest, cheapest paths, an improvement over the prior method of using grid nodes for computing the same algorithms [78]. However for this project CAVER which uses grid nodes was deemed sufficient because supporting programs such as MMC was used for cross correlation.

In CAVER, optimal egress paths from the interior of a protein will connect through points and segments that are furthest from surrounding atoms [78]. The key calculations in CAVER are based on the cost of an edge C(e) given by [78]:

$$C(e) = \frac{l(e)}{d_{closest}(e)^2+\varepsilon} \quad (7)$$

Where l(e) represents the edge length, $d_{closest}$ is the distance from the edge to the closest atom, and ε is a small number to avoid division by zero [78]. Edges are assigned positive values, representing the relative cost of taking each step along a path and considered convenient if it is both sufficiently far from surrounding atoms and sufficiently short [78].

The maximum error introduced by the CAVER algorithm is equal to [$\sqrt{3}/_{(2*d)}$], and the mean error is equal to 0.48 d, where d is the user defined grid resolution [78]. The channel profiles are almost always slightly overestimated by CAVER due to the addition of the mean error, as mentioned above [78]. Upon evaluating CB1 with CP55,940 docked at the orthosteric site, the output images and radii of each channel CAVER identified as an entry and exit are overlaid in a visual representation within the model of CB1. Once the key interaction sites, i.e. the lowest potential binding sites on CB1 for RTI-371 were determined by MMC, CAVER was utilized to identify the molecular channels available for CP55,940 to exit from the activated CB1 protein and directly compared to the outputs from MMC to see where the two intersect.

This process can be summarized in the following steps:

1. Representation of the molecular system under investigation by atom-centered van der Waals spheres
2. Construction of the grid mesh
3. Marking of boundary points by convex hull approximation
4. Optimization of the starting point from a user-defined position
5. Evaluation of edges by a given cost function;
6. Search for the ‘‘cheapest’’ route from the starting point outward on the grid mesh by Dijsktra’s algorithm.

Docking

Results from MMC calculations and Caver were utilized for docking studies. RTI-371’s global minimum conformer was docked at the site identified by MMC calculations and CAVER analysis. These methods had identified this site as most likely because it would block the exit of CP55,940 from the CB1 R* bundle. The docking program, Induced fit (Schrödinger Suite 2011) was used [79-81]. All parameters used for docking and energy minimization were defaults unless otherwise noted. The CB1 R* bundle utilized for docking had CP55,940 docked at the orthosteric site as previously established via mutation studies [43, 68, 82]. Docks were screened for interaction with the ECL2 loop of CB1.

Induced Fit with Rigid Docking

The coordinates of the CB1 R* were prepped for docking using the Protein Preparation Wizard implemented in Maestro (Schrodinger, Inc.). MacroModel (version 9.8) with the OPLS-2005 force field was used for all energy minimizations with water as the fragment. The coordinates of the ligand, RTI-371, were obtained from the global

minimum of the structure previously identified by conformational analysis. Using a starting point dock, based on the results of MMC and Caver, RTI-371 was manually docked such that the tropane ring faced F3.25 and the isoxazole could hydrogen bond to K(183) (ECL1). The N-terminus of CB1 was removed to allow complete access within the ECL region for binding. Rigid receptor–flexible ligand docking calculations were performed using Glide (version 5.7) in XP (extra precision) mode. The induced-fit docking (IFD) protocol implemented in Maestro (version 9.2) was used for flexible receptor docking calculations. The IFD protocol combines Glide docking with Prime (version 3.0) protein structure energy minimization allowing systematic probing of residues within the defined binding pocket space. This protocol allows interactions with the ligand to be maximized and, identified high affinity poses for final docking. Based on this iterative process, multiple poses of the ligand are identified within the three dimensional (3D) box delineated in the input file. Defined around the centroid of the ligand, residues in this box are allowed to relax to accommodate the ligand. Once a predetermined number of ligand–protein complexes were identified, they were docked and minimized as a complex. Finally, the outputs were ranked using the IFD scoring function. The IFD scoring algorithm recognizes favorable hydrophobic, hydrogen-bonding, and metal-ligation interactions, and penalizes steric clashes [83]. The following parameters were used for the IFD protocol. 3D box was 26 Å. This distance was picked specifically to not include the orthosteric ligand, to avoid displacement, but maximize the space within the ECL region around RTI-371. The initial Glide docking was completed

with van der Waals scaling factors of 0.5 for both ligand and receptor. The Prime induced fit refined residues within 5 Å of the ligand and optimized the side chains. The Glide redocking step was performed in XP mode for all structures within 60 kcal/mol of the best, keeping at most 40 structures. For rigid receptor–flexible ligand IFD, the resulting poses were ranked based on IFD Score and XP GScore.

MODELLER

The sixteen removed residues of the N-terminus were replaced and modeled using MODELLER version 9.8. Modeller performs de novo modeling of loops and can be used to identify poses for the N-terminus. Using an alignment sequence with known related structures, MODELLER automatically calculates poses for the N terminus from amino acid sequences containing all non-hydrogen atoms. It implements comparative protein structure modeling by satisfaction of spatial restraints [84-87]. Once the models were visually evaluated and attached to the original bundle, all hydrogen atoms were added on the 16 residue fragment of the N-terminus and the bundle was minimized.

Minimization of bundle with allosteric modulator

The energy of docked RTI-371 allosteric modulator with the CP55,940 in the WT CB1 R* complex was minimized using the OPLS 2005 force field in Macromodel 9.8 (Schrödinger Inc., Portland, OR). An 8.0-Å extended nonbonded cutoff (updated every 10 steps), a 20.0-Å electrostatic cutoff, and a 4.0-Å hydrogen bond cutoff were used in the calculation. A Generalized Born/surface area (GBSA) continuum solvation model for water, or GBSA model, as implemented in Macromodel was used for minimization.

In each minimization the backbone carbons of the transmembrane helix regions and the orthosteric ligand (CP55,940) in the CP55,940 WT CB1 R* complex was treated as non-moving fixed atoms, while the side chains in the transmembrane helix residues and extracellular loop residues were completely free to move. Also, the allosteric modulator RTI-371 was completely free to move, but bond and dihedral angles were constrained to the global minimum conformation during the minimization process. Conjugate gradient minimization was performed for each docked position until a final gradient of 0.05 kcal/mol was reached.

Summary of Methods Used

1. Jaguar – Used to minimize the molecule RTI-371.
2. MMC – Evaluate the free energy of interaction of the fragmented RTI – 371 molecules.
3. Caver – This will evaluate entry and exit route for CP55,940
4. Induced fit - Computational docking of the RTI-371 based on information gained from previous methods
5. Modeler – Replace N terminus post docking allosteric modulator.
6. Macromodel – Minimization of final docks

CHAPTER IV

RESULTS AND DISCUSSION

Conformational Analysis

Three rotatable bonds were identified in RTI-371 and screened for unique low energy conformations. Conformational analysis yielded three resulting minima for RTI-371. (Figure 11) Within the minima, it can be seen that the rotatable bond between the isoxazole and para-chlorobenzene rings yields a high energy cost when rotated and subsequently the two rings remained in plane in all of the low energy conformers. Of the three resulting minima, the conformation with the lowest single point energy of -1558.349352 Hartrees was designated the global minimum. (Figure 11A) Further evaluation of the global min and the second and third low energy minima showed that the two arms of the ligand rotate in concert with one another, thereby eliminating any steric clashes between them. The three minima were all within the 2 kcal/mol of each other and therefore each could have been considered acceptable conformations for docking in CB1. In this case, however, a successful dock was accomplished with the global minimum so the higher energy conformations were not used. The resulting dihedral angles for rotation about Bond 1, Bond 2 and Bond 3, for the global min and two other low energy conformers along with their energies are summarized in Table 3 below.

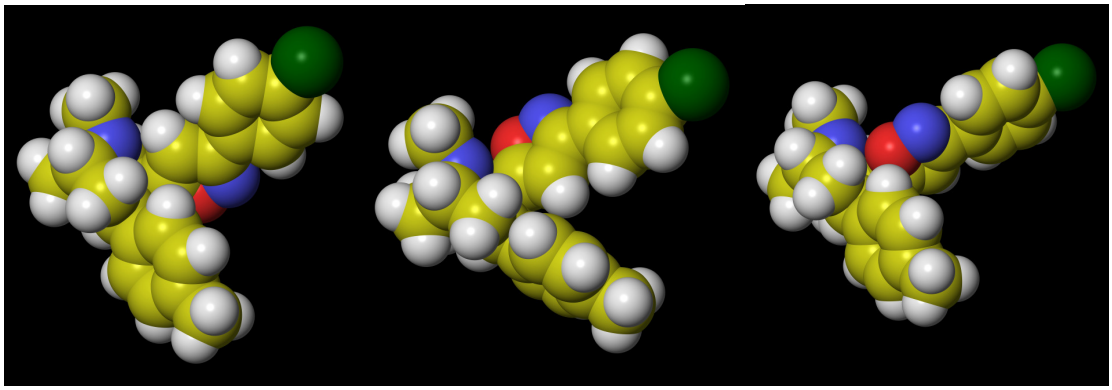

A) Global Minimum **B) Minima 2** **C) Minima 3**

Figure 11: Minima of RTI-371 in VDW with yellow carbons. (A) Global Minimum, (B) Minima 2, (C) Minima 3.

Table 3: Dihedrals of the 3 minima established for RTI-371.

Conformation / Output Number	Dihedral Angle (Bond 1) degrees	Dihedral Angle (Bond 2) degrees	Dihedral Angle (Bond 3) degrees	ΔE kcal/mol
Global Minimum / 829	97.8	179.8	-50.0	0.00000
Minimum 2 / 181	-161.0	2.7	-5.7	0.05481
Minimum 3 / 232	-36.8	0.00	-47.9	1.18251

MMC

Sites at which molecular fragments from RTI-371 (isoxazole and tropane rings and water) have a high affinity for the CB1 (R*)/CP55,940 complex were identified by MMC calculations. In MMC, each B value in the series is held constant until the iterative process of sampling fragment poses is completed, so evaluation of system changes from one B value to the next is important. Specifically, the three key attributes to a successful

MMC run are the following: (1) initially filling the user defined box completely so that the entire CB1 receptor is immersed in the fragment of choice, (2) running long enough to identify a transition state in which the bulk of the fragments have left the cell, and (3) obtaining the minimum B value below which no fragments remain in the box. For Step 1, verification was accomplished two ways; first a visual check was made of the initial snapshot outputs for each of the fragments cited previously, isoxazole, tropane, and water. (Figure 12) For tropane and isoxazole, the 3D defined box is the same size and shape, rectangular with dimensions of 76 x 112 x 76 Å, however, for water it had to be adjusted to 76 x 99 x 76 Å, to avoid having it fill past the upper limit of 20,000 fragment compounds in the MMC program. Visually there was space between the edges of the CB1 bundle and the walls of box and no part of the bundle was outside of the box.

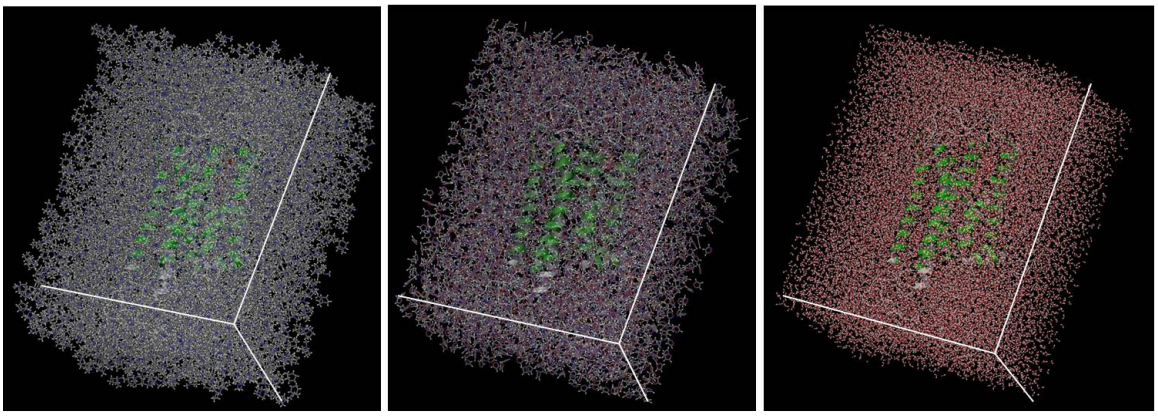

A) Tropane **B) Isoxazole** **C) Water**

Figure 12: Initial Outputs for the fragments for tropane (A), isoxazole (B), and water (C) at high B value.

The minimum number of compounds for each B value can be exported to verify that the key aspects of the MMC are realized. By examining Table 4, the key attribute of filling the box was met because the box was initially filled to >99% for several B values for each of the fragments. This shows that the box was filled and had a chance to stabilize. In the second step, the transition states were realized and can be seen at B value of -4, -2, and -5 for tropane, isoxazole, and water respectively (see Table 4). Visually the bulk of the fragments leave the ensemble at the transition state and each transition state looks different depending on the chemical makeup of the fragment. In the transition state for tropane (hydrophobic) (Figure 13A) the fragments can be seen collecting around the TMH region. This is in contrast to water (hydrophilic) results in which water leaves the TMH region first (Figure 13C). Isoxazole is neither as hydrophobic as tropane nor as hydrophilic as water. Isoxazole hit its transition state first at B = -2 (see Figure 13 B). By visual inspection, it is clear that the isoxazole fragments are dispersed more equally between the ECL (hydrophilic) and TMH (hydrophobic) regions through the transition state.

Finally, the runs were set up to go to values lower B values past the transition state (to B= -13. However, each of the runs terminated due to having no fragment left in the box for any lower chemical potential, thus, the endpoint was identified. Water being present at the lowest B value suggests that it would have to be displaced for a ligand to occupy the same space. Displacing water is considered a thermodynamically favorable move for the whole system as this increases the entropy for the system.

Table 4: Minimum concentration of fragments and correlated percent fill of the 3D box for each MMC run.

B value	Minimum Number of Fragments			% of Box that is Filled		
	Tropane	Isoxazole	Water	Tropane	Isoxazole	Water
3	2487	4710	17896	99.56	99.89	100.00
2	2493	4715	17783	99.80	100.00	99.37
1	2496	4702	17595	99.92	99.72	98.32
0	2498	4648	17208	100.00	98.58	96.16
-1	2497	4501	16581	99.96	95.46	92.65
-2	2486	104	15619	99.52	2.21	87.28
-3	1728	67	13798	69.18	1.42	77.10
-4	31	46	6121	1.24	0.98	34.20
-5	23	37	41	0.92	0.78	0.23
-6	14	27	27	0.56	0.57	0.15
-7	10	18	21	0.40	0.38	0.12
-8	7	15	15	0.28	0.32	0.08
-9	6	10	11	0.24	0.21	0.06
-10	3	6	6	0.12	0.13	0.03
-11	3	4	4	0.12	0.08	0.02
-12	2	4	4	0.08	0.08	0.02
-13	2	3	3	0.08	0.06	0.02

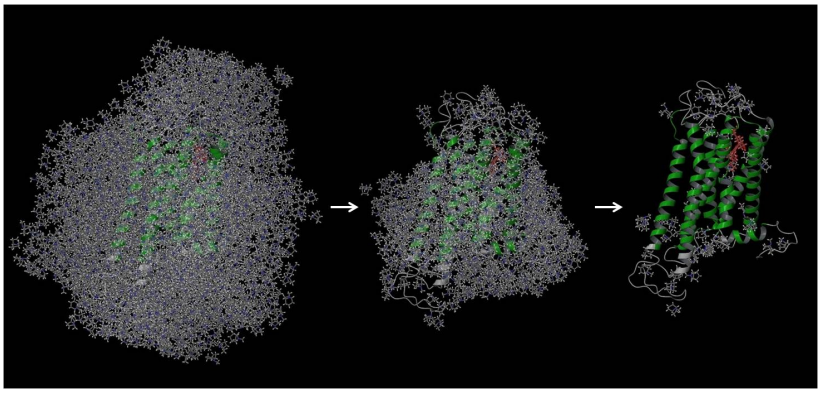

A) Tropane

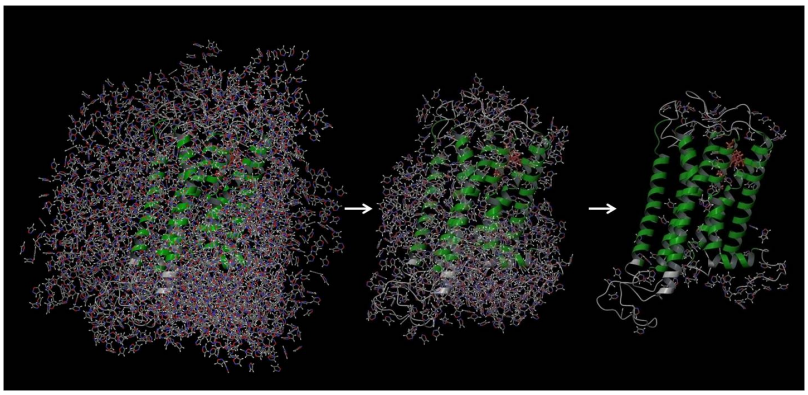

B) Isoxazole

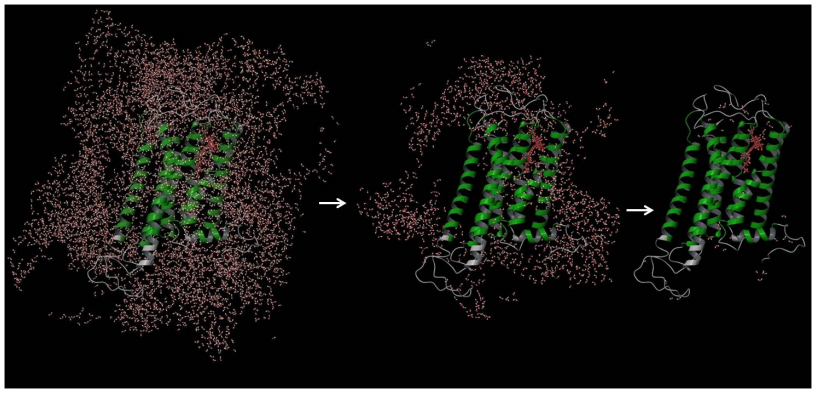

C) Water

Figure 13: Images showing transition state changes for isoxazole (A), tropane (B), and water (C).

Final snapshot outputs for all the fragments at the terminal B value were evaluated to identify where each of these fragments collected. (Figure 14) The locations on the bundle are the same for all the fragments. There are three collection areas, the ICL region at the bottom of the bundle, the TMH region around the orthosteric ligand, and in the ECL region. Since, the G Protein couples at the intracellular end of the bundle, one would expect to have room for fragment collection, but it would not be targeted as an allosteric binding site because it would interfere with G protein coupling. Next, the area around the orthosteric ligand also would not be targeted for binding because allosteric modulators do not displace the orthosteric ligand and docking in this region would ultimately cause this to occur. This, then, leaves the ECL region as the preferred allosteric binding site. This region was previously established as the preferred site by the CAVER analysis (see below).

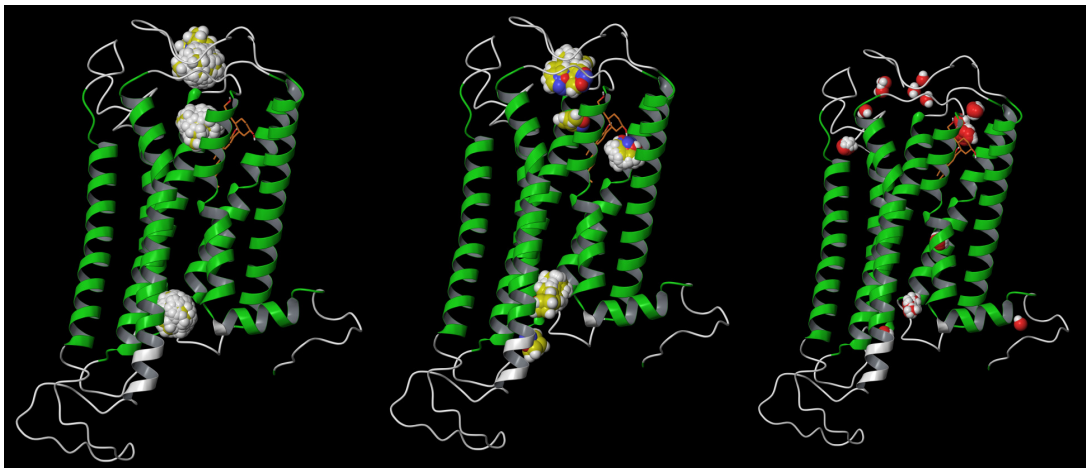

A) Tropane **B) Isoxazole** **C) Water**

Figure 14: Final MMC outputs established for final B value (-3). Overlay of final poses in VDW for each fragment: A) Tropane, B) Isoxazole, and C) Water.

CAVER

Analysis of CB1 R*/CP55,940 complex was performed using CAVER to identify routes of exit for the bound orthosteric ligand CP55,940. The program identified 10 exit tunnels (numbered 0-9 in Table 5) from the binding pocket for CP55,940. In preparation for the CAVER analysis, the bundle was rendered with the ligand removed so there is a cavity in the orthosteric binding pocket. Removal of the ligand is mandatory because its presence will have a high energy cost because the program will identify the space as filled, so removing the ligand yields a better representation of the path out of the bundle. CAVER was set to use a 0.5 Å grid and identify the top 10 tunnels. Of the 10 tunnels identified, only five were unique (Figure 15) and merited individual analysis. Of the 5 unique tunnels, 0, 1, & 5 (purple, orange and red) were unacceptable, because their final exit point from the bundle was into the TMH region (Table 5). Since the most likely exit path of an orthosteric ligand would be through the ECL region, any tunnels that exit through the TMH region are not likely binding sites for allosteric modulation.

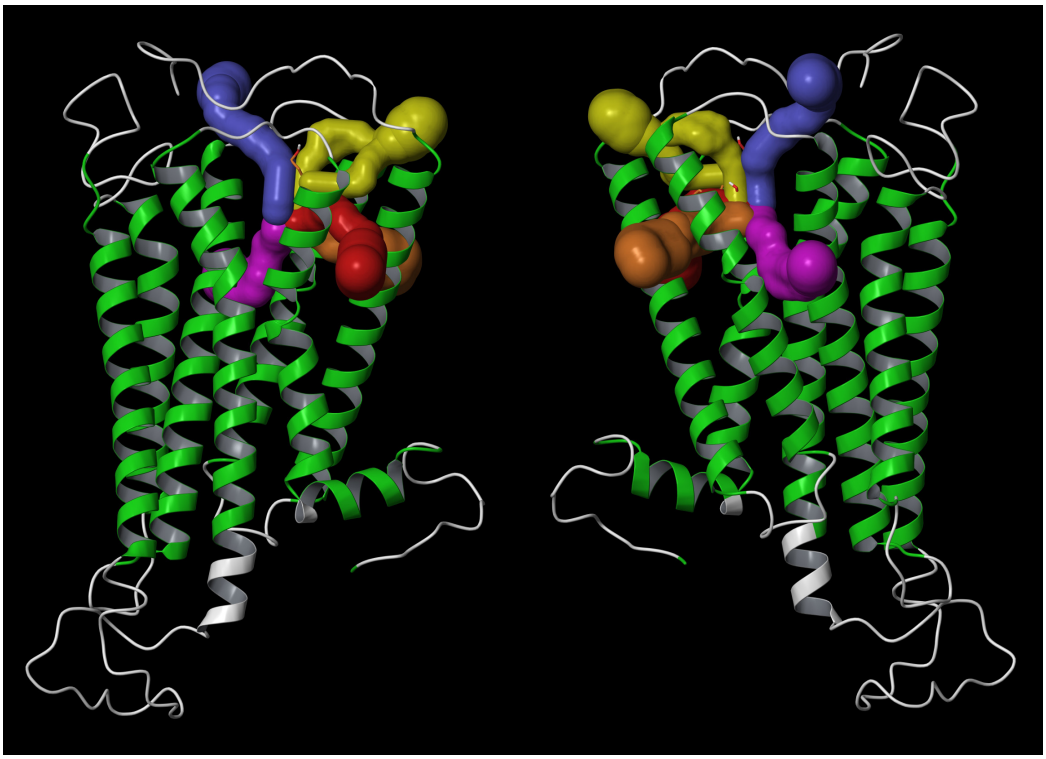

A) Standard View **B) Bundle Rotated 180^{o}**

Figure 15: All tunnels overlaid from CB1 R* CAVER results.

Table 5: Tunnels identified by CAVER

Tunnel	Cost / Length (C_e)	Average Radius (Å)	Length (Å)	Unique	Color in Figure 15	Location
0	12.289	2.3384	46	Yes	Purple	Between TMH2 & 3
1	12.688	2.7354	52	Yes	Orange	Between TMH1 & 2
2	15.158	2.3259	54	No	Purple	Same as Tunnel 0
3	16.586	2.7362	52	No	Orange	Same as Tunnel 1
4	17.071	2.3248	60	Yes	Yellow	Between TMH1 & 2,
5	19.571	2.6040	65	Yes	Red	Between TMH1 & 7
6	19.707	2.3624	63	No	Yellow	Same as Tunnel 4
7	21.388	2.2661	69	Yes	Blue	Between N-ter & ECL1
8	22.593	2.2151	64	No	Yellow	Same as Tunnel 4
9	24.016	2.2791	65	No	Yellow	Same as Tunnel 4

Now of the 10 identified tunnels, 8 were eliminated due to lacking uniqueness and/or exiting in the transmembrane helix region, leaving only 2 tunnels (Figure 16). Investigating the two remaining tunnels showed that only tunnel 7 exits in the proper ECL region. Tunnel 7 shows an exit path above the ECL1, but below the N terminus. Specifically the tunnel would exit CB1 between residues K(183) and R(186) residues above S(185) and D(184). Tunnel 4 was also considered, however, it is in a transitional area at the corner of the ECL and TMH regions making binding of RTI-371 impossible without some of it being in the phospholipid bilayer. A dock with part of the ligand in the bilayer is not typical or likely to occur, lending more evidence against Tunnel 4 as the

potential binding site. Tunnel 7 did meet all of the listed criteria and is the most likely exit route for CP55,940. Identification of this region would accomplish specific aims 2 and 3. It is a region in which MMC showed great affinity for the RTI-371 fragments used (see Figure 14). , Tunnel 7 is coincident with an exit path of the orthosteric ligand, and it resides in an ancillary area to the orthosteric binding pocket ensuring it doesn't compete with the orthosteric ligand.

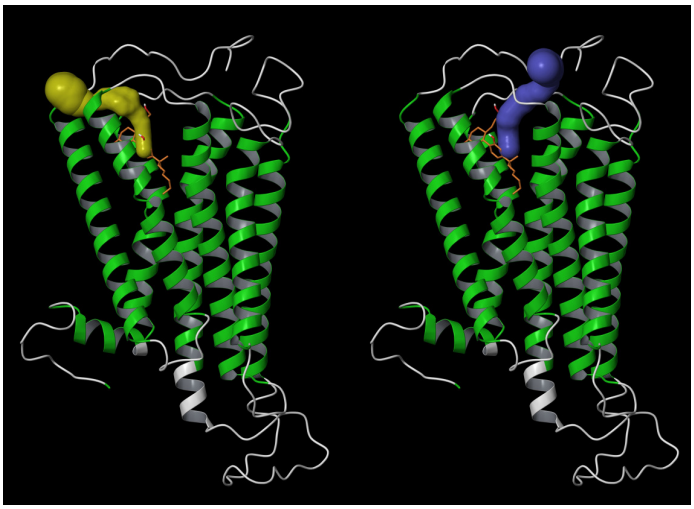

A) Tunnel 4 **B) Tunnel 7**

Figure 16: (a) Caver calculated Tunnel 4 and (B) Caver calculated Tunnel 7 for CB1 R*.

Verification of MMC and CAVER intersection

The final outputs from MMC and CAVER were evaluated to identify key residues that could ultimately define the allosteric binding site and allow for docking RTI-371. To complete this cross correlation, residues within 3Å of the final MMC fragment poses and Tunnel 7 from CAVER were identified. Residues within 3Å of the final B value outputs

for the isoxazole and tropane rings in MMC were K(183), D(184), S(185), R(186), E(258), with isoxazole having one additional residue identified, F(3.25) (see Figure 16A, B). Similarly, the same residues K(183), D(184), and K(373) are found within 3Å of Tunnel 7 from CAVER (Figure 16C). Of the identified residues only D(184) and K(183) are found for all fragments. Given the reoccurrence of these residues, D(184) and K(183) were targeted for initial manual docking of RTI-371 at CB1 (R*), thus accomplishing specific aim 4 of this study.

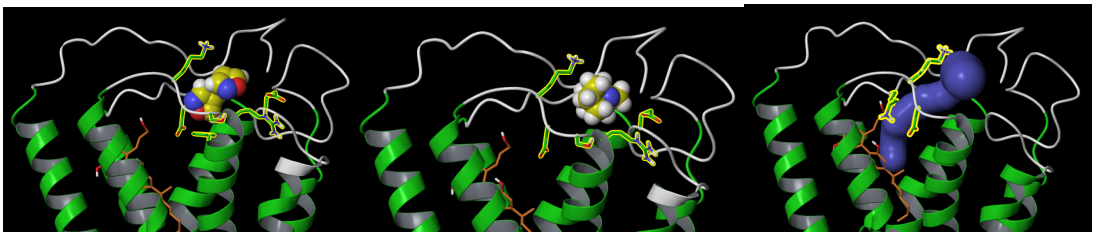

A) Isoxazole **B) Tropane** **C) Tunnel 7**

Figure 17: Residues within 3Å of final isoxazole and tropane poses from MMC and 3Å of Tunnel 7 from CAVER. A) Final isoxazole pose from -3 B Value, B) Final tropane pose from -3 B Value, and C) Tunnel 7.

Final Dock of RTI-371

Initially the allosteric modulator was docked based on the areas previously identified from MMC and CAVER (see Figure 17). Using residue K(183) as a reference, RTI-371 was manually docked near ECL1 with isoxazole hydrogen bonded to K(183), a residue located in the center of the ECL1. In this docked location, the tropane ring faces F(3.25). This manual dock was used as a starting point to run rigid receptor-flexible ligand induced fit docking (IFD) calculations resident as Glide's automated docking

process. The automated docking process yielded two poses and based on the lowest IFD Score and XP GScore (Table 6) the best pose, dock #1, was selected as the preferred, lowest energy allosteric binding site.

Table 6: Glide Scores with critical components from automated docks.

Dock	Scores		Critical Glide Score Components						
	IFD Score	XP GScore	Lipophilic	Hydrogen Bonding	Metal	vdW	Coulomb Energy	RotB	Site
#1	-609.75	-3.04	-0.55	-0.06	0.00	-37.25	-0.79	0.00	0.00
#2	-607.42	-1.35	-0.53	-0.20	0.00	-30.98	-0.50	0.00	-0.02

The conformation of RTI-371 in the final pose was evaluated for its energy relative to the global minimum energy conformation of RTI-371 (see Figure 11, and Table 3). Initially, the docked conformation was found to be ~17 kcal/mol above the global minimum. However, because automatic docking programs can alter ligand conformations in unfavorable ways, the initial docked conformation of RTI-371was replaced with its global minimum energy conformer and the CB1 R*/CP55,940?RTI-371 complex was again minimized in Macromodel using a conjugate gradient minimization to a specific gradient of 0.5 kcal/mol. The final dock and allosteric binding site is based on this energy minimized bundle (Figure 18).

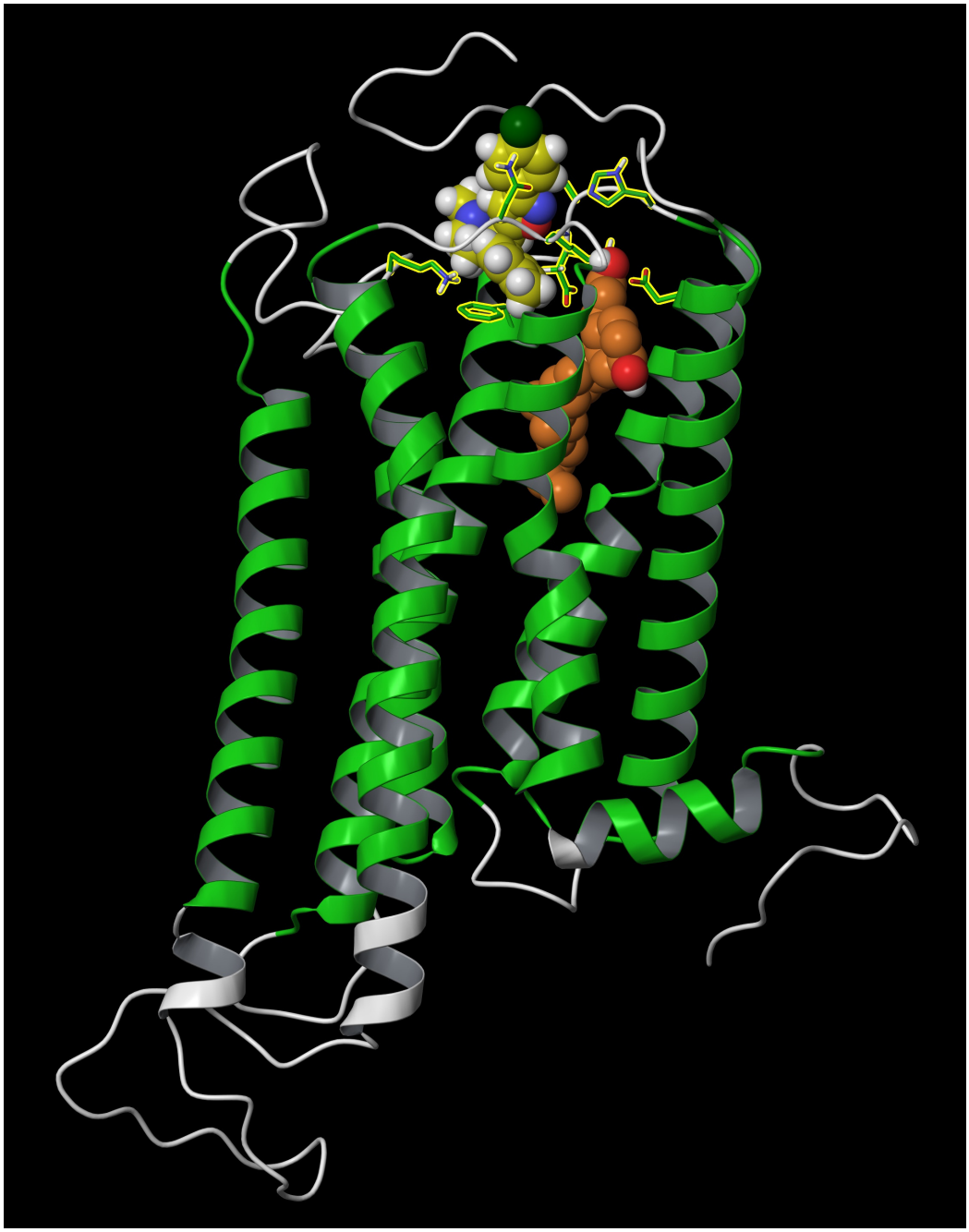

Figure 18: Final dock of the RTI-371 global minimum energy conformer at the identified allosteric site in the ECL region of CB1 R*. Here, the allosteric modulator is shown in yellow, contoured at its in VDW radius. Interacting residues in CB1 R* are outlined in yellow and, the orthosteric ligand, CP55,940, is shown in orange contoured at its VDW radius.

Allosteric Binding Site

The allosteric binding pocket is located in the extracellular region of CB1 (R*) between ECL1 and ECL3. Key residues, interacting with RTI-371 defining its binding site are K(373), N(256), H(181), F(3.25), D(184), K(183), and K(259). The binding pocket for the allosteric modulator is composed of hydrophobic and aromatic interactions, with one hydrogen bond. RTI-371 has no interactions restricting the motion of ECL2, which would interfere with signaling of the CB1 receptor, accomplishing specific aim 5 of this project.

Residues K(373) and D(2.63) in the orthosteric binding pocket were identified as secondary interaction site residues for the orthosteric ligand. These residues form a salt bridge that should not be disturbed by the allosteric modulator. This then insures that there will be no RTI-371competition for the orthosteric binding pocket. Measurement from the terminal H of K(373) to the closest proximity terminal oxygen of D(2.63) measured 1.537 Å suggesting the salt bridge between these residues would still be intact (Figure 19).

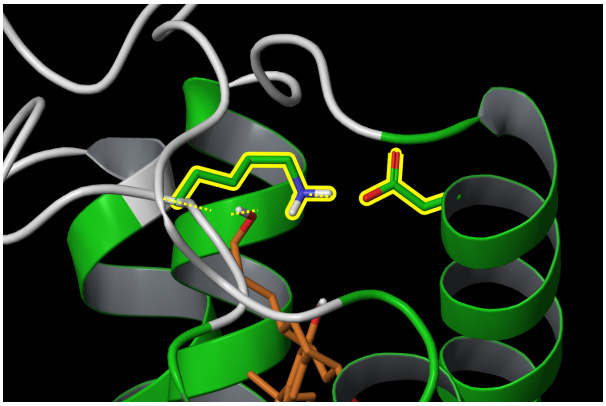

Figure 19: Salt bridge between K (373) (left) and D (2.63) (right) measured at 1.537Å. Figure also shows 2 hydrogen bonds of CP55,940 interacting with K (373).

The binding of RTI-371 near K(183) and D(184) allows RTI-371 to block Tunnel 7 (Figure 20). This supports that the allosteric modulator docked in this site would stabilize the active state of the receptor by blocking the orthosteric ligand from leaving and therefore extending the receptor signaling period.

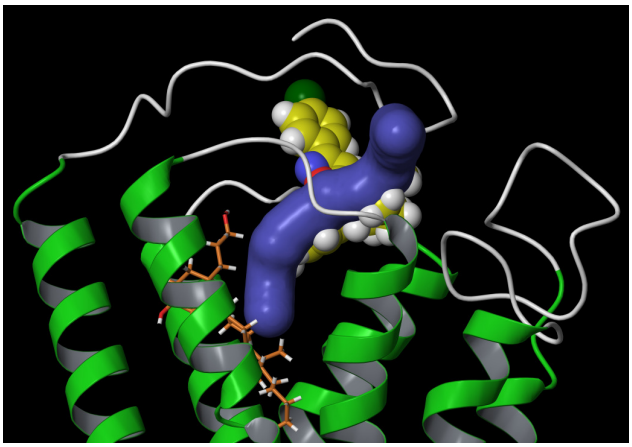

Figure 20: RTI-371 docked at CB1 R* blockings the primary exit, Tunnel 7 as identified by CAVER.

Hydrophobic Interactions

In the allosteric binding site several key residues interact with RTI-371. The allosteric binding site is predominantly in the extracellular loops region and the docked ligand would be in a hydrophilic environment. The water resident in the ECL region will force any hydrophobic-hydrophobic interactions to be quite strong. Oppositely, this same water can shield the hydrogen bonding and weaken its interaction. Figure 21 shows three lysine residues, containing large hydrocarbon segments, participating in hydrophobic packing around RTI-371. These lysine form a pocket surrounding the allosteric ligand. First, K(373) is located between the p-chlorophenyl ring and the methyl benzyl arms of RTI-371. So, when RTI-371 is present, the proximity of K(373) would restrain RTI-371 from freely moving away from the orthosteric ligand, thus assisting in stabilizing the receptor in the active state. Similar hydrophobic packing interactions identified also include K(183) and K(259).

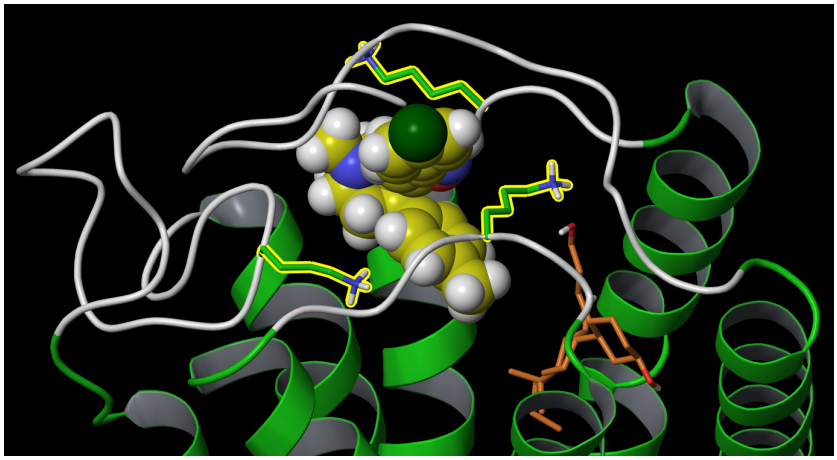

Figure 21: Key hydrophobic residue interactions between RTI 371 and K (373), K (259), and K (183).

Aromatic Interactions

Outside of the hydrophobic interactions, the allosteric binding site also consists of 3 aromatic interactions. At the bottom of Figure 22, a partial aromatic stack exists between F3.25 and methyl benzyl of RTI-371. F3.25 residue provides a floor to the allosteric binding pocket. Also within the three aromatic interacting residues are N(256) and H(181). For N(256) alignment of the δ^- of Cl from p-chlorobenzene with the δ^+ H from N(256) occurs. The δ^- end of H(181) also aligns with the δ^+ edge of the p-chlorobenzene aromatic ring on RTI-371, and this interaction is strengthened by the Cl electron withdrawing group.

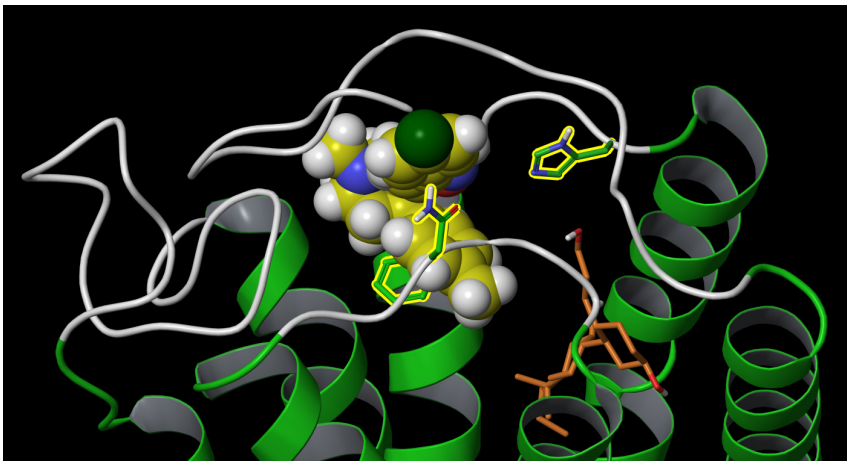

Figure 22: Key aromatic residue interactions between RTI 371 and N (256), H (181), and F3.25

Hydrogen Bonding

Reviewing the other side of RTI-371 for binding interactions reveals a hydrogen bond between the backbone of D(184) and the heteroatom side of the isoxazole ring in RTI-371 (Figure 23). Although normally a hydrogen bond is considered a strong interaction, here it may not be. As stated, the ECL region has water present that can shield a polar interaction.

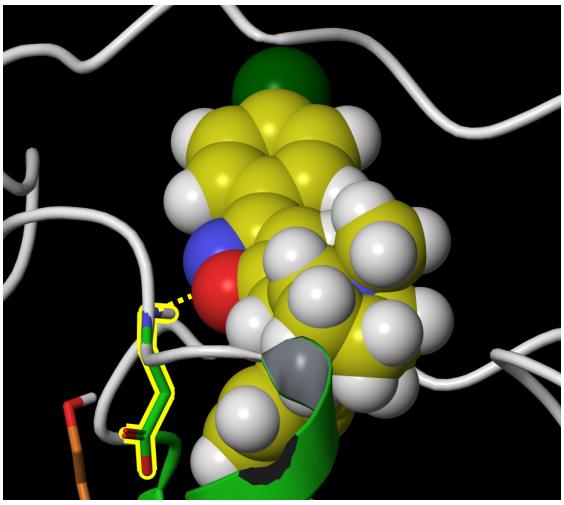

Figure 23: Hydrogen bond between RTI 371 and D (184).

Ultimately, all specific aims of this project were achieved. The global minimum conformation for RTI-371 was established and docked in an area of high affinity based on MMC. The "allosteric" site overlayed with results of CAVER showing RTI-371 would block the exit of CP55,940 from the CB1 R* stabilizing the active state. The final allosteric site stabilizes the between D 2.63 and K (373) salt bridge interaction essential for signaling. This project supports the evidence of positive allosteric modulation for RTI-371 that has been explored and identified through biophysical studies. However, further proof of the allosteric binding sites would need to be verified using RTI-371 with mutation studies using the CB1 receptor.

Positive or negative modulation of receptors such as rhodopsin and more extensively the muscarinic type receptors are typically explored pharmacologically for identification of a compound as a positive or negative modulator. These studies focus on

the increase or decrease in activity based on binding and functional studies. However, very little work on the subject explores identified ligands and their corresponding receptors to identify where allosteric binding occurs in order to develop explanations for why an increase or decrease in activity, depending on the allosteric and orthosteric ligand, occurs. The work here offers a method or template for accomplishing this type of work computationally.

Conclusions

The results from this work support the presence of an allosteric binding site in the extracellular loop region of CB1 R*. Using the global minimum conformation of RTI-371, a dock was established based on sites on the protein surface that have high affinity for fragments of the allosteric modulator. Further evidence suggested that when RTI-371 is docked at this site, it would block an exiting CP55,940. This blockade would hold CP55,940 at its binding site longer and stabilize the CB1 active state. This evidence supports how RTI-371 would act as a positive allosteric modulator as identified from the original biophysical study.

LITERATURE CITED

1. Lundstrom, K., *Structural genomics of GPCRs.* TRENDS in Biotechnology, 2005. **23**(2).
2. Birnbaumer, L., *G proteins in signal transduction.* Annu. Rev. Pharmacol. Toxicol, 1990. **30**: p. 675–705.
3. Matsuda, L.A., Lolait, S.J., Brownstein, M.J., Young, A.C. & BONNER, T.I., *Structure of a cannabinoid receptor: functional expression of the cloned cDNA.* Nature, 1990. **346**: p. 561-564.
4. Abood ME, D.K., Noel MA, et al., *Isolation and expression of a mouse CB1 cannabinoid receptor gene. Comparison of binding properties with those of native CB1 receptors in mouse brain and N18TG2 neuroblastoma cells.* Biochem Pharmacol, 1997. **53**: p. 207-14.
5. Gerard CM, M.C., Vassart G, et al. , *Molecular cloning of a human cannabinoid receptor which is also expressed in testis.* Biochem J., 1991. **279**(pt 1): p. 129-34.
6. Cherezov, V., et al., *High-resolution crystal structure of an engineered human beta2-adrenergic G protein-coupled receptor.* Science, 2007. **318**(5854): p. 1258-65.
7. Rasmussen, S.G., et al., *Crystal structure of the human beta2 adrenergic G-protein-coupled receptor.* Nature, 2007. **450**(7168): p. 383-7.
8. Rosenbaum, D.M., et al., *GPCR engineering yields high-resolution structural insights into beta2-adrenergic receptor function.* Science, 2007. **318**(5854): p. 1266-73.
9. Warne, T., et al., *Structure of a beta1-adrenergic G-protein-coupled receptor.* Nature, 2008. **454**(7203): p. 486-91.
10. Jaakola, V.P., et al., *The 2.6 angstrom crystal structure of a human A2A adenosine receptor bound to an antagonist.* Science, 2008. **322**(5905): p. 1211-7.
11. Wu, B., et al., *Structures of the CXCR4 Chemokine GPCR with Small-Molecule and Cyclic Peptide Antagonists.* Science, 2010. **330**(6007): p. 1066-71.
12. Chien, E.Y., et al., *Structure of the human dopamine d3 receptor in complex with a d2/d3 selective antagonist.* Science, 2010. **330**(6007): p. 1091-5.
13. Palczewski K , K.T., Hori T , et al., *Crystal structure of rhodopsin: a G protein-coupled receptor.* Science, 2000. **289**: p. 739 - 745.
14. Park, J.H., et al., *Crystal structure of the ligand-free G-protein-coupled receptor opsin.* Nature, 2008. **454**: p. 183 - 7.
15. Hanson, M.A. and R.C. Stevens, *Discovery of New GPCR Biology: One Receptor Structure at a Time.* Structure, 2009(17): p. 8 - 14.

16. Cherezov, V., et al., *High-resolution crystal structure of an engineered human beta2-adrenergic G protein-coupled receptor.* Science, 2007. **318**(5854): p. 1258-65.
17. Wu, B., et al., *Structures of the CXCR4 Chemokine GPCR with Small-Molecule and Cyclic Peptide Antagonists.* Science, 2010. **330**(6007): p. 1066-71.
18. Chien, E.Y., et al., *Structure of the human dopamine d3 receptor in complex with a d2/d3 selective antagonist.* Science, 2010. **330**(6007): p. 1091 - 5.
19. Richards, J.E., K.M. Scott, and P.A. Sieving, *Ophthalmology.* 102, 1995: p. 669 - 77.
20. Rana, S. and T.J. Baranski, *Third Extracellular Loop (EC3)-N Terminus Interaction Is Important for Seven-transmembrane Domain Receptor Function: IMPLICATIONS FOR AN ACTIVATION MICROSWITCH REGION.* JOURNAL OF BIOLOGICAL CHEMISTRY, 2010. **285**(41): p. 31472–483.
21. Ye, Y. and A. Godzik, *Flexible structure alignment by chaining aligned fragment pairs allowing twists.* Bioinformatics, 2003. **19**(suppl 2): p. 246 - 55.
22. Okada, T., et al., *The retinal conformation and its environment in rhodopsin.* J. Mol. Biol., 2004. **342**: p. 571 - 83.
23. Vogel, R., et al., *Functional role of the "ionic lock"--an interhelical hydrogen-bond network in family A heptahelical receptors.* J. Mol. Biol., 2008. **380**: p. 648 - 55.
24. Hanson, M.A., et al., *A Specific Cholesterol Binding Site Is Established by the 2.8 Å Structure of the Human β2-Adrenergic Receptor.* Structure, 2008. **16**: p. 897–905.
25. Jaakola, V.P., et al., *The 2.6 angstrom crystal structure of a human A2A adenosine receptor bound to an antagonist.* Science, 2008. **322**(5905): p. 1211-7.
26. Birnbaumer, L., et al., *Studies on the intrinsic activity (efficacy) of human adrenergic receptors. Co-expression of beta 1 and beta 2 reveals a lower efficacy for the beta 1 receptor.* Tex. Heart Inst. J., 1994. **21**(1): p. 16 - 21.
27. Zezula, J. and M. Freissmuth, *The A2A adenosine receptor: a GPCR with unique features?* British Journal of Pharmacology, 2008. **153**: p. 184 - 90.
28. Lomize, M.A., et al., *Orientations of Proteins in Membranes database.* Bioinformatics, 2006. **22**: p. 623 - 25.
29. Ross, R.A., *Allosterism and cannabinoid CB1 receptors: the shape of things to come.* TRENDS in Pharmacological Sciences, 2007. **28**(11): p. 567 - 572.
30. Park, P.S.-H., D.T. Lodowski, and K. Palczewski, *Activation of G Protein–Coupled Receptors: Beyond Two-State Models and Tertiary Conformational Changes.* Annu. Rev. Pharmacol. Toxicol., 2008. **48**: p. 107-141.
31. Goncalves, J.A., et al., *Structure and function of G protein-coupled receptors using NMR spectroscopy.* Progress in Nuclear Magnetic Resonance Spectroscopy, 2010. **57**: p. 159-180.

32. Farrens D , A.C., Ynag K , Hubbell W , Khorana H . *Requirement of rigid-body motion of transmembrane helices for light activation of rhodopsin.* Science, 1996(274): p. 768 - 770.
33. Ghanouni P , S.J., Farrens DL , Kobilka BK, *Agonist induced conformational changes in the G-protein-coupling domain of the beta 2 adrenergic receptor.* Proc Natl Acad Sci USA, 2001(98): p. 5997 - 6002.
34. Lin S , S.T., *Specific tryptophan UV-absorbance changes are probes of the transition of rhodopsin to its active state.* Biochemistry, 1996(35): p. 11149 - 11159.
35. Jensen AD , G.F., Rasmussen SG , Asmar F , Ballesteros JA , Gether U . *Agonist-induced conformational changes at the cytoplasmic side of transmembrane segment 6 in the beta 2 adrenergic receptor mapped by site-selective fluorescent labeling.* J Biol Chem . 2001(276): p. 9279 - 9290.
36. Javitch, J., et al., *Constitutive activation of the beta2 adrenergic receptor alters the orientation of its sixth membrane-spanning segment.* J Biol Chem, 1997. **272**(18549 - 9).
37. Nakanishi, J., et al., *FRET-based monitoring of conformational change of the beta2 adrenergic receptor in living cells.* Biochem Biophys Res Commun., 2006. **343**: p. 1191 - 6.
38. Gether U , L.S., Ghanouni P , Ballesteros J , Weinstein H , Kobilka B, *Agonists induce conformational changes in transmembrane domains III and VI of the beta2 adrenoceptor.* EMBO J, 1997(16): p. 6737 - 6747.
39. Ghanouni Reg* P , S.J., Farrens DL , Kobilka BK, *Agonist induced conformational changes in the G-protein-coupling domain of the beta 2 adrenergic receptor.* Proc Natl Acad Sci USA, 2001(98): p. 5997 - 6002.
40. Altenbach, C., et al., *High-resolution distance mapping in rhodopsin reveals the pattern of helix movement due to activation.* Proc. Natl. Acad. Sci. U.S.A., 2008. **105**: p. 7439 - 7444.
41. Visiers I, E.B., Dracheva S, Ballesteros J, Sealfon SC, and Weinstein H., *Structural motifs as functional microdomains in G-protein-coupled receptors: energetic considerations in the mechanism of activation of the serotonin 5-HT2a receptor by disruption of the ionic lock of the arginine cage.* Int J Quantum Chem, 2002(88): p. 65 - 75.
42. Ballesteros JA , S.L., Javitch JA . *Structural mimicry in G proteincoupled receptors: implications of the high-resolution structure of rhodopsin for structure-function analysis of rhodopsin-like receptors.* Mol Pharmacol . 2001(60): p. 1-19.
43. Ankur Kapur, P.S., Ganesh A. Thakur, Alexandros Makriyannis, and Mary E. Abood, *Mapping the Structural Requirements in the CB1 Cannabinoid Receptor Transmembrane Helix II for Signal Transduction.* JPET, 2007. **325**(1): p. 341-348.

44. McAllister SD , H.D., Barnett-Norris J , Lynch D , Reggio PH , Abood ME . *Structural mimicry in class A G protein-coupled receptor rotamer toggle switches: the importance of the F3.36 201)/W6.48(357) interaction in cannabinoid CB1 receptor activation.* J Biol Chem . 2004(279): p. 48024 - 48037.
45. Guo W , S.L., Filizola M , Weinstein H , Javitch JA . *Crosstalk in G protein-coupled receptors: changes at the transmembrane homodimer interface determine activation.* Proc Natl Acad Sci USA, 2005(102): p. 17495 - 17500.
46. Khanolkar AD, P.S., Makriyannis A, *Molecular probes for the cannabinoid receptors.* Chem Phys Lipids, 2000(108): p. 37 - 52.
47. Kobilka, a.D., *Conformational complexity of G-protein-coupled receptors.* Trends Pharmacol Sci . 2007.
48. Shi L , L.G., Xu R , Guarnieri F , Ballesteros JA , Javitch JA . *Beta 2 adrenergic receptor activation. Modulation of the proline kink in transmembrane 6 by a rotamer toggle switch.* J Biol Chem . 2002(277): p. 40989 - 40996.
49. Borhan B , S.M., Imai H , Shichida Y , Nakanishi K . *Movement of retinal along the visual transduction path.* Science, 2000(288): p. 2209 - 2212.
50. Li J , E.P., Burghammer M , Villa C , Schertler GF . *Structure of bovine rhodopsin in a trigonal crystal form.* J Mol Biol, 2004(343): p. 1409 - 1438.
51. Okada T , F.Y., Silow M , Navarro J , Landau EM , Shichida Y . *Functional role of internal water molecules in rhodopsin revealed by X-ray crystallography.* Proc Natl Acad Sci USA, 2002. **99**: p. 5982 - 5987.
52. Singh R , H.D., Barnett-Norris J , Lynch DL , Reggio PH , Guarnieri F . *Activation of the cannabinoid CB1 receptor may involve a W6.48/F3.36 rotamer toggle switch.* J Pept Res, 2002(60): p. 357 - 370.
53. Karnik, S.S., et al., *Activation of G-proteincoupled receptors: a common molecular mechanism.* Trends Endocrinol. Metab., 2003. **14**: p. 431 – 7.
54. Davidson, F.F., P.C. Loewen, and H.G. Khorana, *Structure and function in rhodopsin: replacement by alanine of cysteine residues 110 and 187, components of a conserved disulfide bond in rhodopsin, affects the light-activated metarhodopsin II state.* Proc. Natl. Acad. Sci. USA 1994. **91**: p. 4029 - 33.
55. Zeng, F.Y., et al., *Conserved extracellular cysteine pair in the M3 muscarinic acetylcholine receptor is essential for proper receptor cell surface localization but not for G protein coupling.* . J. Neurochem. , 1999. **72**: p. 2404 - 14.
56. Cook, J.V. and K.A. Eidne, *An intramolecular disulfide bond between conserved extracellular cysteines in the gonadotropin-releasing hormone receptor is essential for binding and activation.* Endocrinology, 1997. **138**: p. 2800 - 06.
57. Klco, J.M., et al., *Essential role for the second extracellular loop in C5a receptor activation.* Nature Structural & Molecular Biology, 2005. **12**(4): p. 320 - 26.
58. Klco, J.M., et al., *Essential role for the second extracellular loop in C5a receptor activation.* Nature Structural & Molecular Biology, 2005. **12**(4): p. 320 - 26.

59. Ahuja, S., et al., *Helix movement is coupled to displacement of the second extracellular loop in rhodopsin activation.* NATURE STRUCTURAL & MOLECULAR BIOLOGY, 2009. **16**(2): p. 168 - 75.
60. Palczewski, K., et al., *Crystal structure of rhodopsin: a G protein-coupled receptor.* Science, 2000. **289**: p. 739 - 745.
61. Sgourakis, N.G. and A.E. Garcia, *The Membrane Complex between Transducin and Dark-State Rhodopsin Exhibits Large-Amplitude Interface Dynamics on the Sub-Microsecond Timescale: Insights from All-Atom MD Simulations.* J. Mol. Biol., 2010. **398**: p. 161 - 173.
62. Herrmann, R., et al., *Signal Transfer from GPCRs to G Proteins ROLE OF THE G alpha N-TERMINAL REGION IN RHODOPSIN-TRANSDUCIN COUPLING.* JOURNAL OF BIOLOGICAL CHEMISTRY, 2006. **281**(40): p. 30234 - 30241.
63. Hamm, H.E., *Minireview: The Many Faces of G Protein Signaling.* JOURNAL OF BIOLOGICAL CHEMISTRY, 1998. **273**(2): p. 669 - 672.
64. Filipek, S., et al., *A concept for G protein activation by G protein-coupled receptor dimers: the transducin/rhodopsin interface.* P h o t o c h e m . P h o t o b i o l . S c i, 2004. **3**: p. 628 - 638.
65. Wall, M.A., et al., *The structure of the G protein heterotrimer Gi alpha 1 beta 1 gamma 2.* Cell (Cambridge,Mass.), 1995. **83**: p. 1047-1058.
66. Reggio, P., *Computational Methods in Drug Design: Modeling G Protein-Coupled Receptor Monomers, Dimers, and Oligomers.* The AAPS Journal, 2006(8): p. 322-336.
67. Balabin, I.A., W. Yang, and D.N. Beratan., *Coarse-grained modeling of allosteric regulation in protein receptors.* Proc. Natl. Acad. Sci. USA, 2009. **106**: p. 14253 - 58.
68. McAllister, S., et al., *An aromatic microdomain at the cannabinoid CB1 receptor constitutes an agonist/inverse agonist binding region.* J Med Chem, 2003(46): p. 5139-5152.
69. Hurst, D.U., U.; Lynch, D.; Seltzman, H.; Hyatt, S.; Roche, M.; McAllister, S.; Fleischer, D.; Kapur, A.; Abood, M.; Shi, S.; Jones, J.; Lewis, D.; Reggio, P., *Biarylpyrazole inverse agonists at the cannabinoid CB1 receptor: importance of the C-3 carboxamide oxygen/lysine3.28(192) interaction.* J Med Chem, 2006(49): p. 5969 - 5987.
70. Barnett-Norris, J., Hurst, D. P., Buehner, K., Ballesteros, J. A., Guarnieri, F. and Reggio, P. H., *Agonist alkyl tail interaction with cannabinoid CB1 receptor V6.43/I6.46 groove induces a helix 6 active conformation.* International Journal of Quantum Chemistry, 2002. **88**(1): p. 76 - 86.
71. Song Z-H, a.B.T., *A lysine residue of the cannabinoid receptor is critical for receptor recognition by several agonists but not WIN55212-2.* Mol Pharmacol. Ther, 1996(49): p. 891-896.

72. Chin C, A.V., Lucas-Lenard J, and Kendall D, *Ligand binding and modulation of cyclic AMP levels depends on the chemical nature of residue 192 of the human cannabinoid receptor 1.* J Neurochem, 1998. **70**: p. 366 - 373.
73. Brizzi A, C.M., Brizzi V, Bisogno T, Dinatolo MT, Martinelli A, Tuccinardi T, Di Marzo V., *Design, synthesis, binding, and molecular modeling studies of new potent ligands of cannabinoid receptors.* Bioorg Med Chem, 2007. **15**(16): p. 5406 - 5416.
74. Navarro, H.A., et al., *Positive allosteric modulation of the human cannabinoid (CB1) receptor by RTI-371, a selective inhibitor of the dopamine transporter.* British Journal of Pharmacology, 2009. **156**(7): p. 1178 - 1184.
75. Leach, A.R., *Conformational Analysis*, in *Molecular Modeling, Principles and Applications*. 2006, Pearson Education Limited. p. 458 - 464.
76. Schrödinger , L., *Jaguar*. 2005: New York, NY.
77. Clark, M., et al., *Grand Canonical Monte Carlo Simulation of Ligand-Protein Binding*. J. Chem. Inf. Model, 2006. **46**: p. 231 - 242.
78. Petřek, M., et al., *MOLE: A Voronoi Diagram-Based Explorer of Molecular Channels, Pores, and Tunnels.* Structure, 2007. **15**(11): p. 1357 - 1363.
79. Schrödinger, *Suite 2011 Induced Fit Docking protocol; Glide version 5.7, Schrödinger, LLC, New York, NY, 2011; Prime version 3.0, Schrödinger, LLC, New York, NY,*. 2011.
80. Sherman, W., et al., *Novel Procedure for Modeling Ligand/Receptor Induced Fit Effects.* J. Med. Chem., 2006. **49**(534).
81. Sherman, W., H.S. Beard, and R. Farid, *Use of an Induced Fit Receptor Structure in Virtual Screening.* Chem. Biol. Drug Des, 2006. **67**: p. 83.
82. Picone RP, K.A., Xu W, Ayotte LA, Thakur GA, Hurst DP, Abood ME, Reggio PH, Fournier DJ, and Makriyannis A, *(-)-7'-Isothiocyanato-11-hydroxy-1',1'-dimethylheptylhexahydrocannabinol (AM841), a high-affinity electrophilic ligand, interacts covalently with a cysteine in helix six and activates the CB1 cannabinoid receptor.* Mol Pharmacol . 2005. **68**: p. 1623 - 1635.
83. Eldridge, M.D., et al., *Empirical scoring functions: I. The development of a fast empirical scoring function to estimate the binding affinity of ligands in receptor complexes.* J. Comput.-Aided Mol. Des., 1997. **11**: p. 425-445.
84. Sali, A. and T.L. Blundell, *Comparative protein modelling by satisfaction of spatial restraints.* J. Mol. Biol., 1993. **234**: p. 779-815.
85. A. Fiser, R.K. Do, and A. Sali., *Modeling of loops in protein structures.* Protein Science, 2000. **9**: p. 1753-1773.
86. Eswar, N., et al., *Comparative Protein Structure Modeling With MODELLER.* Current Protocols in Bioinformatics, 2006. **Supplement 15**: p. 5.6.1-5.6.30.
87. Marti-Renom, M.A., et al., *Annu. Rev. Biophys. Biomol. Struct.* Comparative protein structure modeling of genes and genomes, 2000. **29**: p. 291-325.